# CONTINUOUS BEAM PHOTOELECTRON SPECTROSCOPY OF CLUSTER ANIONS

S. T. ARNOLD, J. G. EATON, D. PATEL-MISRA, H. W. SARKAS, and K. H. BOWEN*

## 1. INTRODUCTION

The study of gas-phase cluster anions provides an avenue for addressing open questions in topics as diverse as ion solvation, excess electrons in fluids, ion-molecule reactions, ion-induced nucleation, and electronic band structure in solids. In the past, experimental investigations of negative cluster ions have included thermochemical (ref. 1-3), kinetic (ref. 4), electron attachment (ref. 5,6), and spectroscopic studies, with the latter exploring total photodestruction (ref. 7,8), photodissociation (ref. 9,10), and photodetachment (ref. 11) processes. At the same time, theoretical studies have dealt with the related topics of negative ion solvation (ref. 12-14), trapped and solvated electron states (ref. 15,16), and the variation of metal cluster electron affinities with cluster size (ref. 17-19).

In recent years, dramatic progress in the photodetachment of electrons from negative cluster ions and related anionic species has been occurring in several laboratories. Using pulsed negative ion photoelectron spectroscopy, Smalley and his colleagues (ref. 20-27) have recorded the spectra of $C^-_{n=2\text{-}30,48\text{-}84}$, $Cu^-_{n=6\text{-}41}$, $Ag^-_{n=3\text{-}21}$, $Au^-_{n=2\text{-}21}$, $Nb^-_{n=4\text{-}12}$, $Pb^-_{n=2\text{-}12}$, $Si^-_{n=3\text{-}20}$, $Ge^-_{n=3\text{-}15}$, $Sn^-_{n=2\text{-}12}$, and $Al^-_{n=3\text{-}32}$; Johnson's group (ref. 28-31) has measured the spectra of $(O_2)^-_{n=2\text{-}6}$, $O_2^-(N_2)_1$, $NO^-(NO)_1$, $(CO_2)^-_{n=2\text{-}13}$, $O_2^-(H_2O)_1$, and $NO_2^-(N_2O)_1$; Neumark et al. (ref. 32-34) have recorded the spectra of $(ClHCl)^-$, $(IHI)^-$, $(BrHBr)^-$, $(FHCl)^-$, and $(BrHCl)^-$; and Meiwes-Broer and his colleagues (ref. 35-39) have taken the spectra of $Al^-_{n=2\text{-}25}$, $Ag^-_{n=3\text{-}22}$, $Ni^-_{n=3\text{-}18}$, $Sn^-_{n=2\text{-}20}$, $Pb^-_{n=2\text{-}20}$, $Pd^-_{n=2\text{-}22}$, $Bi^-_{n=2\text{-}15}$, and $Mg^-_{n=3\text{-}10}$. Using ion cyclotron resonance photodetachment spectroscopy, Brauman and his coworkers (ref. 40-42) have investigated a variety of solvated anions of the form $(ROHF)^-$. Using continuous beam negative ion

photoelectron spectroscopy, Lineberger's group (ref. 43-51) has measured the spectra of $Cu^-_{n=2-10}$, $Fe_2^-$, $Co_2^-$, $Ag^-_{n=2-6}$, $Re_2^-$, $Ni^-_{n=2-8}$, $Pd_3^-$, $Pt^-_{n=2,3}$, $(Na_mF_n)^-$, $Fe(CO)^-_{n=1-4}$, $Ni(CO)^-_{n=1-3}$, $H^-(H_2O)_1$, and $D^-(D_2O)_1$; Ellison et al. (ref. 52), have taken the spectrum of $Si_2^-$; and in our laboratory (ref. 53-59) we have recorded the photoelectron spectra of $NO^-(N_2O)_{n=1-5}$, $H^-(NH_3)_{n=1,2}$, $D^-(ND_3)_1$, $NH_2^-(NH_3)_{n=1,2}$, $ND_2^-(ND_3)_{n=1,2}$, $NO^-(Ar)_1$, $NO^-(Kr)_1$, $NO^-(Xe)_1$, $O_2^-(Ar)_1$, $NO^-(H_2O)_{n=1,2}$, $NO^-(D_2O)_{n=1,2}$, $(CO_2)_2^-$, $(N_2O)_2^-$, $(CS_2)_2^-$, $(SO_2)_2^-$, $(H_2O)^-_{n=2,6,7,10-25,30,34,37,40}$, $(D_2O)^-_{n=2,6,7,11-23}$, $Ar(H_2O)^-_{n=2,6,7}$, $Ar(D_2O)^-_{n=2,6,7}$, $Ar_2(D_2O)_6^-$, $Na^-_{n=2-5,7}$, $K^-_{n=2-7}$, $Rb^-_{n=2-4}$, $Cs^-_{n=2,3}$, $(NaK)^-$, $(Na_2K)^-$, $(KRb)^-$, $(KCs)^-$, $(K_2Cs)^-$, and $(RbCs)^-$. Clearly, progress in cluster anion photodetachment spectroscopy has been rapid, and the field is beginning to flourish across a chemically diverse range of systems.

This chapter primarily surveys recent advances in continuous beam photoelectron (photodetachment) spectroscopy of negative cluster ions and related anionic species. Recent developments in pulsed beam photoelectron spectroscopy of metal and semiconductor cluster anions are described in the companion chapter by O. Cheshnovsky, C. L. Pettiette, and R. E. Smalley. Our chapter is organized as follows. Experimental methods employed in continuous beam photoelectron spectroscopy are described in section two which discusses these and highlights several of the more important continuous beam cluster ion sources. The remaining three sections survey selected cluster anion studies. Section three deals with ion-molecule complexes, systems in which the excess negative charge is localized on a single component of the cluster anion. Section four considers molecular cluster anions which exhibit excess charge delocalization, these systems being exemplified by water cluster anions. Lastly, section five surveys continuous beam studies of metal cluster anions including transition metal and alkali metal systems.

## 2. EXPERIMENTAL METHODS

### 2.1 Spectrometer

Continuous beam negative ion photoelectron spectroscopy is conducted by crossing a steadily-operating beam of mass-selected negative ions with a continuous, fixed-frequency photon beam and energy analyzing the resultant photoelectrons. Following the pioneering experiments of Hall, this technique was developed and brought to maturity by Lineberger with important



contributions by Ellison and by Hotop (ref. 60,61). Over the past few years, the technique has begun to be applied to investigate negative cluster ions. A typical continuous beam negative ion photoelectron spectrometer (ref. 62) is shown in Figure 1. Its main components are: an ion beam line along which negative ions are formed, transported, and mass-selected; a continuous, fixed-frequency photon source capable of achieving high power in the ion-photon interaction region; and a magnetically shielded, high resolution electron energy analyzer.

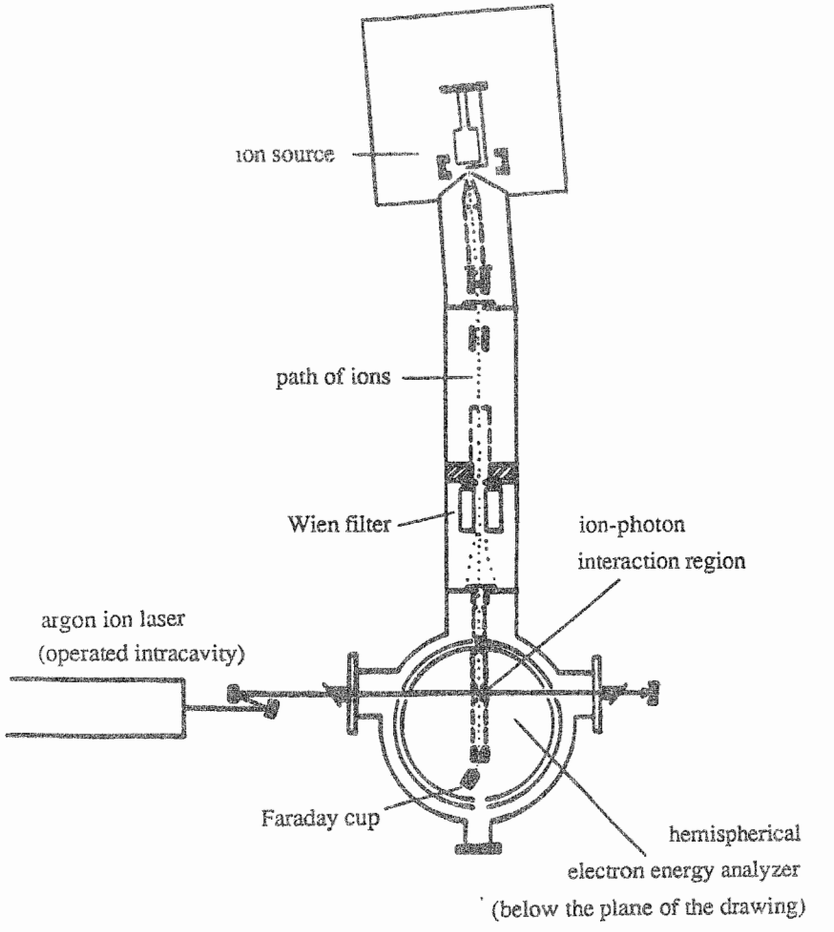


Figure 1. Schematic diagram of a typical continuous beam negative ion photoelectron spectrometer

The first element of the beam line is the negative ion source (see Section 2.2). Next comes a series of electrostatic lenses, usually cylindrical but in some apparatus quadrupolar, which are designed to extract ions from the ion source and transport them through the mass selector to the ion-photon interaction region. Along the way, the ions are bent through a small angle in order to eliminate ultraviolet photons and electronic metastables emanating from the source. The mass selector functions as a sample purifier allowing the selection of a particular cluster anion mass prior to its interaction with the photon beam. This is a particularly important experimental attribute since it allows interference-free photoelectron spectra to be obtained. While any mass selector compatible with continuous beam techniques may be employed, devices exhibiting high ion transmission with good ion optical quality are preferred due to the high ion intensities and tight ion focal properties required by this technique. The device most commonly used is an E×B mass separator (a Wien velocity filter) because, in addition to these properties, it also possesses a simple straight-through geometry. The primary shortcoming of the Wien filter is its modest mass resolution.

The continuous, high power photon source required by this technique is provided by modern laser technology. Because they can easily deliver high powers (~100 circulating W) of visible photons (~2.5 eV) when operated intracavity in the ion-photon interaction region, argon ion lasers have been the workhorses of continuous beam negative ion photoelectron spectroscopy. Visible photons provide sufficient energy to photodetach many negative ions and negative cluster ions. There are other anionic species, however, where the use of higher energy ultraviolet photons is necessary. In this area, the work of Smalley and his coworkers has been especially noteworthy. Since high power ultraviolet lasers tend to be pulsed, the technique of pulsed beam negative ion photoelectron spectroscopy has been particularly well suited to ultraviolet studies. Recently, however, new developments have also extended ultraviolet capability to continuous beam experiments. Utilizing an external cavity buildup system, Lineberger and coworkers (ref. 63) have converted the relatively weak outputs of an argon ion laser in the near-ultraviolet to an equivalent of ~40 W in the ion-photon interaction region. This new development has thereby opened the door to investigating cluster anions in the ultraviolet by continuous beam negative ion photoelectron spectroscopy.

The remaining component of a negative ion photoelectron spectrometer is its magnetically shielded electron energy analyzer. The continuous beam technique couples well to electrostatic



electron energy analyzers. Because they achieve the best combination of electron transmission efficiency and resolution, hemispherical electrostatic analyzers have most often been employed in this technique. By sampling a small solid angle of the photodetached electrons, hemispherical electron energy analyzers can achieve resolutions that range from 5-50 meV. Good resolution in an electron energy analyzer is indispensable when investigating vibrational structure or closely spaced electronic states.

## 2.2 Ion Sources

Until the last several years, the application of negative ion photoelectron spectroscopy to cluster anions was impeded by a lack of adequate cluster anion sources. Ideally, the solution to this void in ion source technology would be a single, universal cluster anion source. Such a universal source would be capable of producing high intensity beams of internally cold cluster ions while exhibiting good ion optical properties. In addition, such a device would possess complete chemical versatility, being able to produce a wide array of atomic and molecular cluster anions. Although no universal source of cluster ions has emerged, the goals of such a device have, to a large extent, been met collectively by the development of several kinds of cluster ion sources. Developments in pulsed cluster anion sources are covered in the chapter by R. E. Smalley and his coworkers. Below, we describe several of the continuous cluster anion sources that have been used in negative ion photoelectron spectroscopy.

A flow tube ion source has been utilized by Lineberger and coworkers to produce and study several negative cluster ions. In this device, ions and cluster ions generated near one end of a tube are entrained in an excess of inert gas and are made to flow, due to a pressure drop, toward the other end where some of them pass through a sampling orifice into the spectrometer. Flow tubes tend to be particularly well-behaved ion sources, attributes being the collisional thermalization of their ions and the provision of rational synthetic routes for ion production. Thus far, Lineberger has used two methods of ionization to produce cluster anions, namely microwave and dc cold cathode discharges (ref. 47,48). In the former, a small amount of precursor material, eg. such as $Re_2(CO)_{10}$, is introduced into the helium flow slightly downstream of the microwave discharge. Cluster ions are formed by the reaction of the precursor with the plasma and these are entrained in the viscous flow of

helium. Figure 2 shows a schematic of the flow tube cluster ion source outfitted with a dc cold cathode discharge for ionization. When using the dc cold cathode discharge, a small amount of argon is introduced into the helium carrier gas. Argon cations produced in the discharge sputter the cathode which is composed of the metal to be studied. The metal atoms and clusters formed by sputtering then interact with the plasma to yield anions which in turn form cluster anions by ion-molecule reactions during their trek down the tube. Both versions of this source have been used for the generation of transition metal cluster anions.

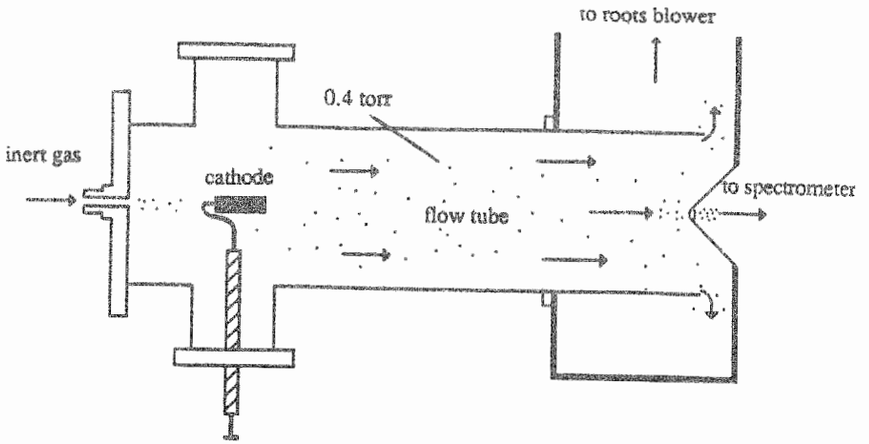


Figure 2. Schematic diagram of the flow tube cluster ion source

Supersonic jet expansion cluster ion sources are a versatile means of generating cool, intense, and chemically diverse beams of cluster ions. In our laboratory, we have utilized both high and low temperature sources of this type to generate a wide variety of cluster anions. The low temperature source (for gaseous feedstocks) is similar in spirit to that developed by Haberland (ref. 64). In our version of this source (see Figure 3), gas at a high pressure is expanded through a pinhole aperture into a high vacuum, while a negatively biased hot filament injects low energy electrons directly into the expanding jet in the presence of a magnetic field (ref. 55). The effect is to implant low energy electrons into a highly condensation-prone environment. There, the primary electrons collide with the expansion gas producing even lower energy secondary electrons which are probably the prime agents of electron attachment. The resultant beam is then skimmed, and the ions are extracted into



the spectrometer. Examples of cluster anions which we have generated with this source include $H^-(NH_3)_n$, $NO^-(N_2O)_n$, and $(H_2O)_n^-$. An alternate method of ionization has been used by Lineberger and coworkers who crossed the jet expansion with a tightly focussed electron beam.

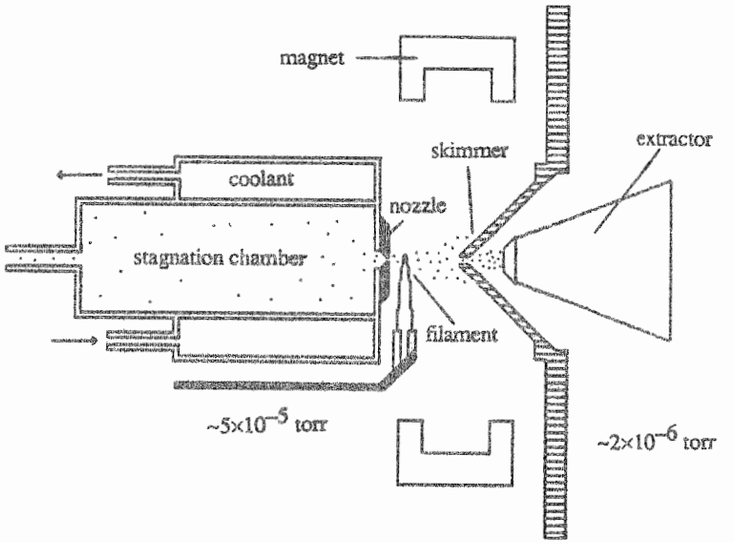


Figure 3. Schematic diagram of the low temperature supersonic expansion cluster ion source

The high temperature version of our supersonic expansion cluster anion source is shown in Figure 4. In this source, the stagnation chamber is divided into separately heated oven reservoir and nozzle channel sections. This source operates by heating a sample in the oven region to a temperature corresponding to several torr equilibrium vapor pressure. The vapor is then coexpanded with several hundred torr of argon into high vacuum through a nozzle channel which is maintained ~50 degrees hotter than the oven. Electrons are injected into the expanding jet by an ionization scheme similar to that used in the low temperature expansion source. The resultant cluster ions are then skimmed by a heated skimmer and extracted into the spectrometer. We have generated both homogeneous and heterogeneous alkali metal cluster anions in this manner.

The recent development (ref. 65) of the nucleation-based "smoke-ion" source in our laboratory represents a promising new advance in continuous cluster ion source technology. This device is

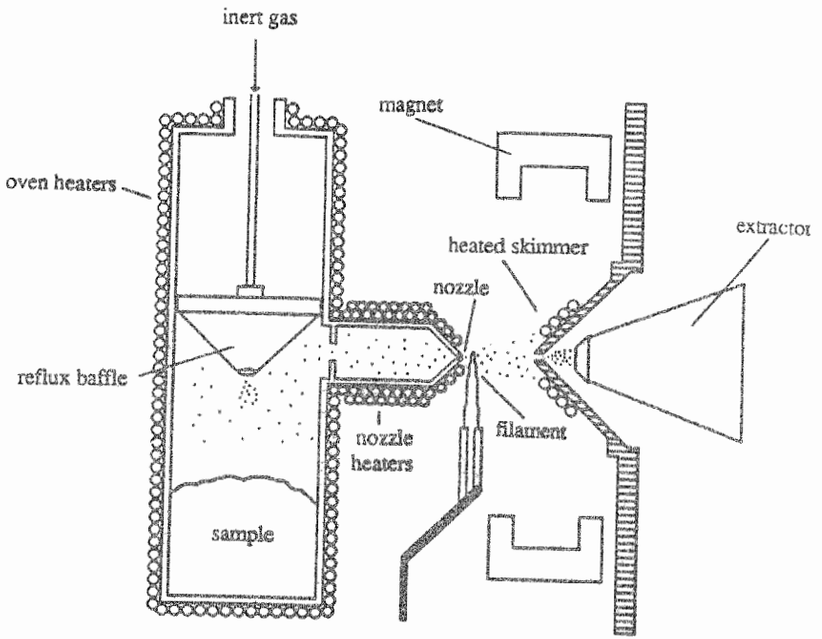


Figure 4. Schematic diagram of the high temperature supersonic expansion ion source

capable of generating intense beams of large cluster ions from relatively high temperature materials. The "smoke-ion" source (see Figure 5) is the result of combining inert gas condensation methods with techniques for injecting electrons into expanding jets. In this source, a resistively heated oven evaporates the material of interest into a cool inert gas condensation cell. In this environment, the evaporated material nucleates to form a dilute smoke composed of ultrafine particles and clusters. A small aperture allows the inert gas, along with its entrained smoke, to exit the cell into the high vacuum region via a weak jet expansion. A negatively biased hot filament placed on the high vacuum side of the aperture injects low energy electrons into the high density portion of the expanding jet inducing the formation of cluster ions from the entrained particles, hence the name "smoke-ion" source. The resulting beam is skimmed, and the cluster ions are extracted and transported to the spectrometer. In preliminary mass spectral studies using lead and lithium, large ion beam currents of both positive and negative cluster ions were observed. The corresponding cluster size distributions



detected in each case ranged from n=1-400 for $Pb_n^+$ and $Pb_n^-$ and from n=12-5,700 for $Li_n^-$. Future developmental efforts will be directed toward higher temperature materials. We anticipate that this source will be useful in several pursuits, among them continuous beam photoelectron spectroscopy of cluster anions.

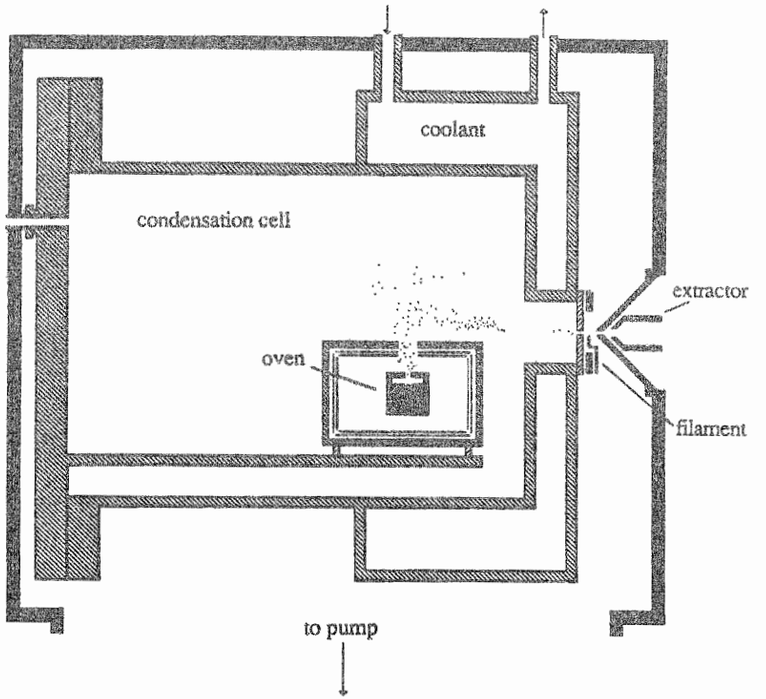


Figure 5. Schematic diagram of the "smoke-ion" source

## 3. ION-MOLECULE COMPLEXES: CLUSTER ANIONS WITH LOCALIZED EXCESS CHARGES

The nature of cluster anion bonding is closely related to the issue of how excess negative charges are distributed over their cluster anions. One can imagine two limiting cases for such charge distributions. In the simplest case, the system's excess negative charge localizes itself on a specific component of the cluster anion to form a sub-ion which interacts with the remaining neutral components. In the other case, the excess negative charge is dispersed over all or part of the cluster

anion. The former localized charge case describes simple ion-molecule complexes which are the focus of this section, while cluster anions exhibiting excess charge delocalization are discussed in section four. Ion-molecule complexes are reminiscent of the usual notion of a solvated anion in which a central negative ion is surrounded by a sheath of neutral solvent molecules. As the number of solvent molecules within the complex increases, the energetic properties of the ion-molecule system evolve from those of the free ion toward those of a solvated anion in solution. Consequently, the study of these localized charge systems contributes to our understanding of interatomic and intermolecular phenomena in the size regime between single atomic or molecular species and the condensed phase.

The energetic relationships between the generic ion-molecule complexes, $X^-(Y)_n$, and their corresponding neutral clusters, $X(Y)_n$, are expressed through the identities,

$$EA[X(Y)_n] = EA[X] + \sum_{m=0}^{n-1} D[X^-(Y)_m\cdots Y] - \sum_{m=0}^{n-1} D_{WB}[X(Y)_m\cdots Y] \quad (1)$$

and

$$EA[X(Y)_n] = EA[X(Y)_{n-1}] + D[X^-(Y)_{n-1}\cdots Y] - D_{WB}[X(Y)_{n-1}\cdots Y], \quad (2)$$

where $EA[X(Y)_n]$ denotes the adiabatic electron affinity of the $X(Y)_n$ cluster, $D[X^-(Y)_m\cdots Y]$ is the ion-neutral dissociation energy (the absolute value of the solvation energy) for the loss of a single neutral solvent, Y, from a given negative cluster ion, and $D_{WB}[X(Y)_m\cdots Y]$ is the weak-bond dissociation energy for the loss of a single solvent, Y, from a given neutral cluster. Since ion-solvent interaction energies generally exceed van der Waals bond strengths, it is evident from these relations that clustering can be expected to stabilize the excess electronic charge on a negative ion and that the electron affinities of clusters should increase, at least up to a point, with cluster size.

Negative ion photoelectron spectroscopy provides an important means of studying these ion-molecule complexes. The photoelectron spectroscopic experiments described here map out both stepwise ion-solvent dissociation energies (sequential solvation energies) and electron affinities as functions of cluster size. Also, in some cases, complexation-induced structural distortions in these ion-solvent complexes are revealed in their photoelectron spectra. The photoelectron spectra of ion-molecule complexes may be roughly viewed as the spectra of their perturbed sub-ions. Typically, the main features in the spectra of ion-molecule complexes resemble those of their



uncomplexed sub-ions except for their being broadened and shifted to higher electron binding energies due to the stabilizing effect of solvation. The electron binding energy of the sub-ion's shifted origin peak is the adiabatic electron affinity of the cluster, while the electron binding energy of the maximum in the sub-ion's shifted spectral envelope is taken to be the vertical detachment energy of the cluster anion. The magnitude of the spectral shift gives an approximate value for the ion solvation energy of the complex. And, when a spectral feature appears which is attributable to the complexation-induced structural distortion of the neutral solvent by its sub-ion, the relative intensity of this feature is a measure of the extent to which the solvent molecule has been distorted.

Below, we present short descriptions of several selected studies of ion-molecule complexes. We start with the ion-molecule complexes, $H^-(NH_3)_{n=1,2}$ before proceeding to discuss $NH_2^-(NH_3)_{n=1,2}$ and $H^-(H_2O)_1$. We then present a series of ion-molecule studies involving the sub-ion, $NO^-$, beginning with the series $NO^-(Ar)_1$, $NO^-(Kr)_1$, and $NO^-(Xe)_1$, and continuing with $NO^-(N_2O)_{n=1-5}$, and then with $NO^-(H_2O)_{n=1,2}$. While the emphasis of this chapter is on continuous beam photoelectron spectroscopy of cluster anions, ion-molecule complexes have also been investigated via pulsed beam photoelectron spectroscopy and ion cyclotron resonance photodetachment. Owing to the importance of these contributions, several examples of ion-molecule complexes studied by these techniques are also presented below. In particular, we present two ion-molecule studies involving the sub-ion, $O_2^-$, before concluding this section with investigations of ion-molecule complexes of the form $(ROHF)^-$.

### 3.1 $H^-(NH_3)_{n=1,2}$

The hydride ion-ammonia complex has long been implicated in liquid ammonia solutions as an intermediate in the proton transfer reaction

$$NH_2^- + H_2 \rightleftharpoons H^- + NH_3 \quad (3)$$

The first observation of $NH_4^-$ in the gas phase, however, did not occur until 1982 when Nibbering and coworkers (ref. 66) generated it in a Fourier transform ion cyclotron spectrometer via the reaction

$$HCO^- + NH_3 \rightarrow CO + NH_4^- \quad (4)$$

Deuterium labeling experiments demonstrated that all of the hydrogen atoms in $NH_4^-$ were not equivalent, and these investigators concluded that $NH_4^-$ is comprised of a hydride ion solvated by an

ammonia molecule, ie. $H^-(NH_3)_1$.

Of the cluster anions studied thus far by negative ion photoelectron spectroscopy, $H^-(NH_3)_1$ is currently the most thoroughly investigated by theoretical methods. The first calculations on $H^-(NH_3)_1$ were performed twenty years ago by Ritchie and King (ref. 67). More recently, ab initio computations on $NH_4^-$ have also been carried out by Rosmus et al. (ref. 68), by Squires (ref. 69), by Schleyer and colleagues (ref. 70), by Cremer and Kraka (ref. 71), by Cardy et al. (ref. 72), by Hirao and Kawai (ref. 73), and by Ortiz (ref. 74); all of whom agree that the most stable configuration of $NH_4^-$ is an $H^-(NH_3)_1$ ion-dipole complex in which the hydride ion is bound at a relatively long distance to only one of ammonia's hydrogens almost collinearly with a N–H bond of ammonia. In addition to a hydrogen-bonded $NH_4^-$ ion-molecule complex, calculations by Schleyer et al. (ref. 70), by Cremer and Kraka (ref. 71), by Cardy and colleagues (ref. 72), and by Ortiz (ref. 74) also find a bound, higher energy, nitrogen-bonded $NH_4^-$ isomer of tetrahedral symmetry. Recent ab initio calculations on double Rydberg molecular anions by Simons and his colleagues (ref. 75) find a tetrahedral $NH_4^-$ as well.

The ion-molecule complexes, $H^-(NH_3)_1$ and $H^-(NH_3)_2$, were generated in our laboratory using ammonia in a supersonic expansion ion source, and they were photodetached with 2.540 eV photons (ref. 53,59). Their photoelectron spectra, shown in Figure 6, are both dominated by large peaks which have been designated as peaks A and A', respectively. The $H^-(NH_3)_1$ spectrum also exhibits a smaller peak on the low electron kinetic energy side of peak A which is labeled as peak B. The shoulder on the low electron kinetic energy side of peak A' in the $H^-(NH_3)_2$ spectrum is marked as peak B'. A much smaller third peak also exists in the $H^-(NH_3)_1$ spectrum, and this is designated as peak C. Its analog does not appear in the $H^-(NH_3)_2$ spectrum. Below, these spectral features are each discussed in turn.

As previewed above, the main features in these spectra resemble the spectrum of the free hydride ion, except for being broadened and shifted to higher electron binding energies. Thus, peaks A and A' are both due to the photodetachment of solvated hydride ion "chromophores" within $H^-(NH_3)_1$ and $H^-(NH_3)_2$, and the shifts are a consequence of the hydride sub-ions being stabilized by their interactions with ammonia solvent molecules. The electron binding energy of the center of peak A in the $H^-(NH_3)_1$ spectrum is 1.109 eV. In addition to being the vertical detachment energy of $H^-(NH_3)_1$, this value is also a good estimate of and an upper limit to both the dissociative



detachment energy of $H^-(NH_3)_1$ and the electron affinity of $H(NH_3)_1$. Likewise, the electron binding energy of peak A' in the $H^-(NH_3)_2$ spectrum is 1.455 eV, and it is similarly interpreted. An upper limit to the ion-solvent dissociation energy of $H^-(NH_3)_1$ breaking into $H^-$ and $NH_3$ is

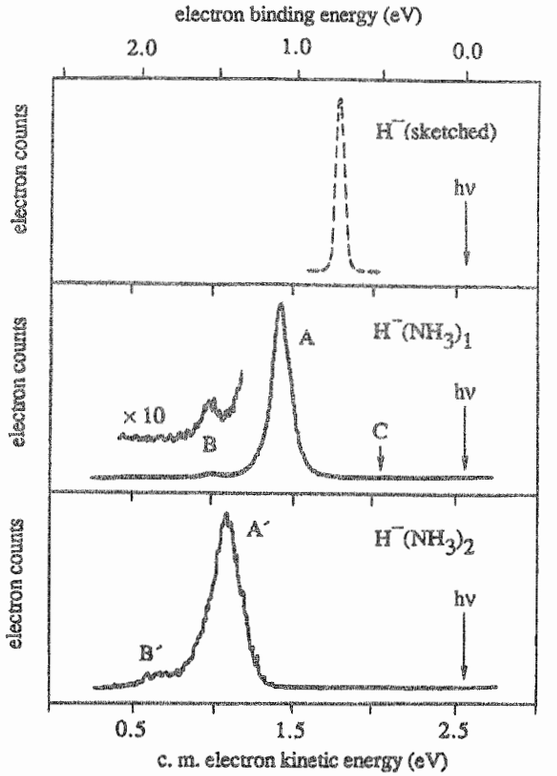


Figure 6. Photoelectron spectra of $H^-(NH_3)_1$ and $H^-(NH_3)_2$. The spectrum of $H^-$ is a single peak, and it has been sketched here for comparison.

given by subtracting the electron affinity of H (0.754 eV) from the vertical detachment energy of $H^-(NH_3)_1$, ie. the spectral shift between peak A in the spectrum of $H^-(NH_3)_1$ and the lone peak in the spectrum of $H^-$. This value is 0.36 eV, and it is in good agreement with most theoretical calculations for the ion-solvent dissociation energy of $H^-(NH_3)_1$. In a similar manner, the ion-single solvent dissociation energy of $H^-(NH_3)_2$ breaking into $H^-(NH_3)_1$ and $NH_3$ is given by subtracting the vertical detachment energy of $H^-(NH_3)_1$ from that of $H^-(NH_3)_2$, ie. the shift between peaks A

and A'. The value of this second solvation energy is 0.35 eV, close to that of the first solvation energy.

Peak B in the spectrum of $H^-(NH_3)_1$ arises due to the complexation-induced distortion of the ammonia solvent by its $H^-$ sub-ion. The center of peak B is separated from that of peak A by 3480 $cm^{-1}$ in the $H^-(NH_3)_1$ spectrum, and by 2470 $cm^{-1}$ in the $D^-(ND_3)_1$ spectrum. These energy differences are very close to the stretching frequencies of $NH_3$ and $ND_3$, indicating that peak B is due primarily to the excitation of a stretching mode in the ammonia solvent during photodetachment The intensity of peak B is a measure of the extent to which the ammonia solvent molecule has been perturbed. The small Franck-Condon factor that is observed suggests that the ammonia is only slightly distorted upon complexation with the hydride ion in $H^-(NH_3)_1$. The B' shoulder in the $H^-(NH_3)_2$ spectrum arises in an analogous way.

The $H^-(NH_3)_1$ spectrum also contains a much smaller third feature (peak C), and the experimental evidence (ref. 59) implies that it arises due to the photodetachment of a higher energy $NH_4^-$ isomer of tetrahedral structure. This isomer is not a cluster, and it is best described as a double Rydberg molecular anion comprised of a $NH_4^+$ core with two diffuse electrons.

### 3.2 $NH_2^-(NH_3)_{n=1,2}$

In a related study (ref. 57), we also recorded the photoelectron spectra of the amide ion-ammonia complexes, $NH_2^-(NH_3)_1$ and $NH_2^-(NH_3)_2$. These spectra are presented in Figure 7 along with the photoelectron spectrum of $NH_2^-$ which is presented for comparison. The spectra of $NH_2^-(NH_3)_1$ and $NH_2^-(NH_3)_2$ are both dominated by large peaks which are labeled as A and A', respectively. In the spectrum of $NH_2^-(NH_3)_1$ a less intense feature, peak B, appears on the low electron kinetic energy side of peak A. Again, the dominant peaks in both spectra arise due to the photodetachment of solvated sub-ion "chromophores" within the cluster ions. In these cases, the sub-ions are amide ions, and again with further solvation the dominant peak shifts to progressively higher electron binding energies due to the stabilizing effect of solvation. The center of peak A in the $NH_2^-(NH_3)_1$ spectrum corresponds to an electron binding energy of 1.30 eV, and as previously described, this is the vertical detachment energy of $NH_2^-(NH_3)_1$ as well as a good estimate of the electron affinity. The electron binding energy of peak A' in the $NH_2^-(NH_3)_2$ spectrum is 1.78 eV.



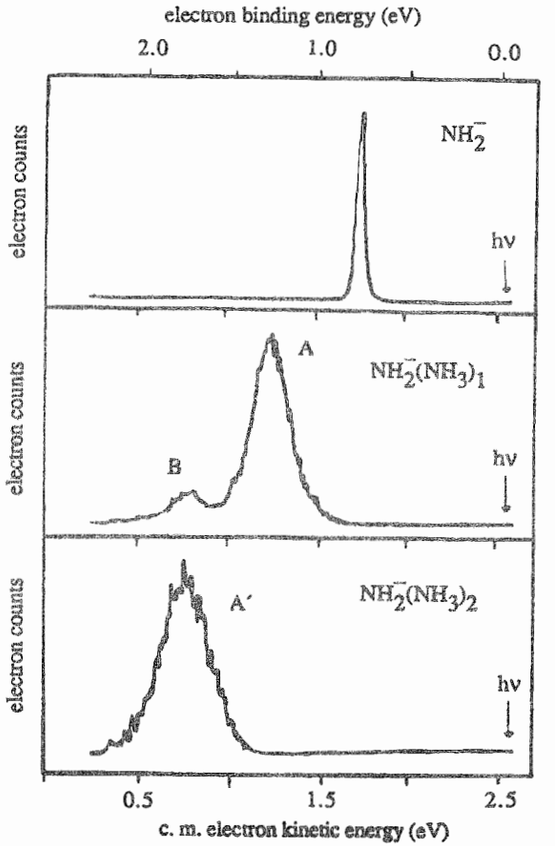


Figure 7. Photoelectron spectra of $NH_2^-$, $NH_2^-(NH_3)_1$, and $NH_2^-(NH_3)_2$

and it is similarly interpreted. An upper limit to the ion-solvent dissociation energy of $NH_2^-(NH_3)_1$ breaking into $NH_2^-$ and $NH_3$ is given by the difference in energy between the center of the $NH_2^-$ spectral peak and the center of peak A in the $NH_2^-(NH_3)_1$ spectrum. This value is 0.52 eV, and it is in good agreement with theoretical calculations by Squires (ref. 69). Likewise, the ion-single solvent dissociation energy of $NH_2^-(NH_3)_2$ breaking into $NH_2^-(NH_3)_1$ and $NH_3$ is given by the difference in energy between the centers of peaks A and A' in the cluster ion spectra. This value is 0.48 eV indicating an approximately equal stabilization of $NH_2^-$ by both the first and second ammonia solvent molecules. Peak B in the photoelectron spectrum of $NH_2^-(NH_3)_1$ is separated from peak A by an energy corresponding to an ammonia stretching frequency, just as in the $H^-(NH_3)_1$ spectrum. This

peak is primarily due to the excitation of a stretching mode in the ammonia solvent during photodetachment, and its relative intensity is a measure of the extent to which the ammonia solvent is distorted due to its complexation with the amide anion. The isotope shift in the photoelectron spectrum of $ND_2^-(ND_3)_1$ also supports this interpretation.

The photoelectron spectra of $H^-(NH_3)_{n=1,2}$ and $NH_2^-(NH_3)_{n=1,2}$ are qualitatively similar. Both H and $NH_2$ have essentially identical electron affinities, and in these systems both $H^-$ and $NH_2^-$ are solvated by ammonia. Also, all four spectra exhibit dominant peaks which arise due to the photodetachment of electrons from sub-ion chromophores within their cluster ions. Furthermore, the $H^-(NH_3)_1$ and $NH_2^-(NH_3)_1$ spectra both exhibit smaller peaks to the low electron kinetic energy side of their main peaks, and in both cases the A-B energy spacings correspond to ammonia stretching frequencies. Quantitatively, however, the two systems are rather different. The $NH_2^-(NH_3)_{n=1,2}$ spectra both exhibit larger shifts and more broadening than the $H^-(NH_3)_{n=1,2}$ spectra. The first and second ion-solvent dissociation energies for both $NH_2^-(NH_3)_1$ and $NH_2^-(NH_3)_2$ are ~0.5 eV, while those for $H^-(NH_3)_1$ and $H^-(NH_3)_2$ are both ~0.35 eV. Clearly, the interaction of $NH_2^-$ with ammonia is stronger than that of $H^-$ with ammonia in these complexes. This is also consistent with the fact that the relative intensity of peak B is larger in the $NH_2^-(NH_3)_1$ spectrum than in the $H^-(NH_3)_1$ spectrum. In addition, calculations by Squires (ref. 69) found that the ammonia N–H bond which interacts with the anion is more elongated in $NH_2^-(NH_3)_1$ than in $H^-(NH_3)_1$.

Using flow tube techniques to study the reaction, $NH_2^- + H_2 \rightarrow H^- + NH_3$, Bohme has shown that $NH_2^-$ is a stronger base than $H^-$ in the gas-phase (ref. 76). This suggests that the higher ion-solvent dissociation energy of $NH_2^-(NH_3)_1$ relative to $H^-(NH_3)_1$ may be a consequence of $NH_2^-$ being a stronger base than $H^-$. The clustering of solvent molecules around a bare gas-phase anion stabilizes the excess negative charge on the ion, and this results in a decrease in its gas-phase basicity. Often, the relative ordering of basicities in the gas-phase is found to be the reverse of their ordering in solution. A comparison of these two cluster anion systems allowed us to determine the degree of solvation required to cause this ordering to switch over. By using the ion-solvent dissociation energies determined from our spectra in appropriate thermochemical cycles, we were able to calculate the relative basicities of $NH_2^-$ vs. $H^-$, $NH_2^-(NH_3)_1$ vs. $H^-(NH_3)_1$, and $NH_2^-(NH_3)_2$ vs. $H^-(NH_3)_2$. A plot of basicity vs. solvation number revealed that a reversal in the



relative ordering of basicities in these systems occurs by the addition of the second ammonia solvent to these ions.

### 3.3 $H^-(H_2O)$

Lineberger and his coworkers (ref. 45) have recorded the photoelectron spectra of $(H_3O)^-$ and $(D_3O)^-$. These species were prepared in a flow tube ion source by reacting hydroxide anions with formaldehyde. The spectra demonstrate that $(H_3O)^-$ and $(D_3O)^-$ are ion-molecule complexes of the form $H^-(H_2O)$ and $D^-(D_2O)$. The photoelectron spectrum of $D^-(D_2O)$ is presented in Figure 8. It and its $H^-(H_2O)$ analog exhibit features which are analogous to those observed in the ion-molecule spectra discussed previously. In particular, the $D^-(D_2O)$ spectrum is dominated by a single peak with a less intense peak on its low electron kinetic energy side. The main spectral feature resembles that of $H^-$ except for being broadened and shifted to higher electron binding energy. Consequently,

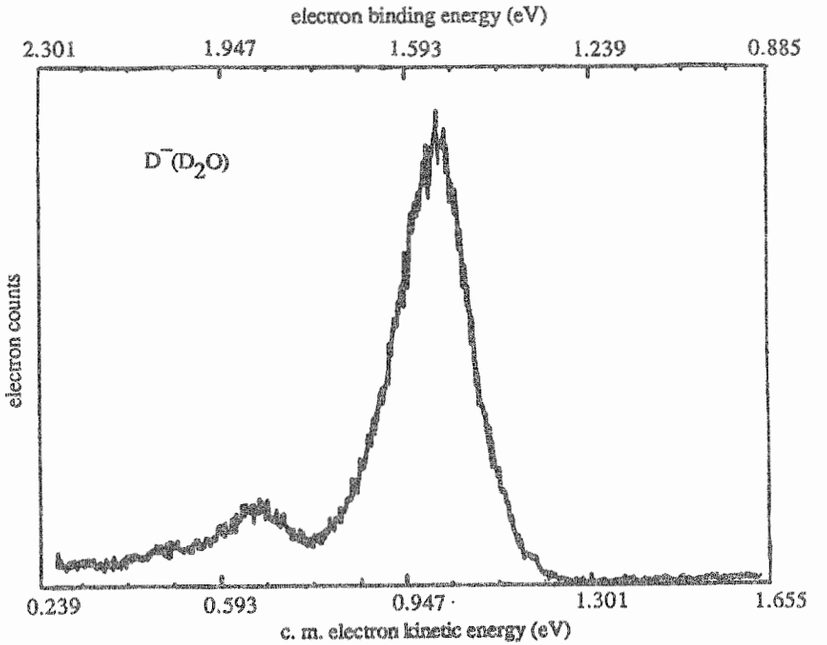


Figure 8. Photoelectron spectrum of $D^-(D_2O)$

this peak is interpreted as arising from the photodetachment of a solvated hydride sub-ion within $H^-(H_2O)$. From the spectrum, a vertical electron detachment energy of 1.52 eV is obtained, and as in the previous cases, this value is probably a reasonable approximation to the electron affinity of the neutral cluster. Since the electron affinity of H is 0.754 eV while that of OH is 1.83 eV, the vertical detachment energy determined for $(H_3O)^-$ indicates that it is $H^-(H_2O)$ rather than $OH^-(H_2)$. By subtracting the electron affinity of H from the vertical detachment energy, the ion-solvent dissociation energy of $H^-(H_2O)$ breaking into $H^-$ and $H_2O$ was estimated to be 0.8 eV. For comparison, recall that an ion-solvent dissociation energy of 0.36 eV was obtained for $H^-(NH_3)$, illustrating that the interaction between $H^-$ and water is about twice as strong as that between $H^-$ and ammonia.

In both the $H^-(H_2O)$ and the $D^-(D_2O)$ spectra, the smaller peak provides evidence that the neutral water solvents have been distorted due to complexation, as observed in the previous examples. The less intense peak in the spectrum is separated from the dominant peak by the energy of the asymmetric stretching frequency of water, indicating that this spectral feature is due to the excitation of an asymmetric stretching mode in the water solvent during photodetachment. This distortion is consistent with a hydrogen bonded structure for the hydride ion-water complex.

### 3.4 $NO^-(Ar)$, $NO^-(Kr)$, $NO^-(Xe)$

A variety of interactions are involved in the bonding of ion-molecule complexes. Comparing systems having the same neutral solvents affords the opportunity of examining differences in ion-molecule bonding which stem from complexation with various sub-ions. Previously, such a comparison was made between the related species. $NH_2^-(NH_3)_n$ and $H^-(NH_3)_n$. Alternatively, however, ion-molecule bonding may also be examined by comparing systems with identical sub-ions but with different solvent molecules. With this in mind, we have studied a family of ion-molecule complexes all containing nitric oxide sub-ions. These include ion-molecule complexes in which a nitric oxide anion is solvated by rare gas atoms, by nitrous oxide molecules, and by water molecules.

The photoelectron spectra of $NO^-(Ar)_1$, $NO^-(Kr)_1$, and $NO^-(Xe)_1$, presented in Figure 9 (ref. 57), are highly structured and clearly exhibit spectral patterns which resemble the photoelectron spectrum of $NO^-$. The vibrational structure observed in the $NO^-$ spectrum is retained in the spectra of the rare gas (Rg) nitric oxide anion complexes with the individual peaks slightly broadened and



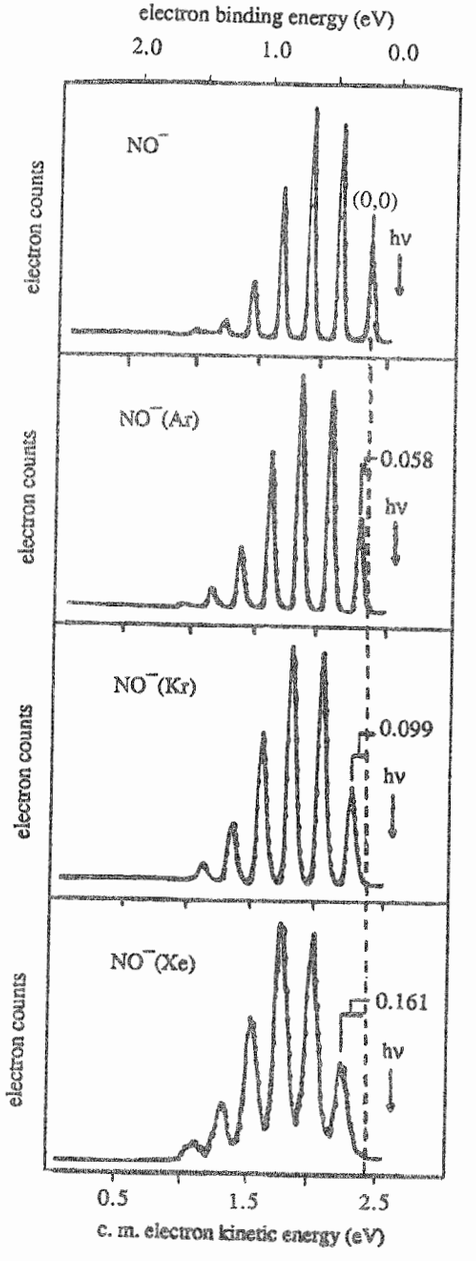


Figure 9. Photoelectron spectra of $NO^-$, $NO^-(Ar)$, $NO^-(Kr)$, and $NO^-(Xe)$

with their vibrational envelopes shifted to higher electron binding energies. Thus, each of these spectra is interpreted in terms of a largely intact $NO^-$ sub-ion which is solvated and stabilized by a rare gas atom. Approximate electron affinity values were determined from the difference between the photon energy and the electron kinetic energy of the origin peak in a given $NO^-(Rg)$ spectrum. These values were found to be 0.095 eV, 0.136 eV, and 0.204 eV for the argon, krypton, and xenon complexes, respectively. All of these complexes are rather weakly bound. The ion-solvent dissociation energy for a particular $NO^-(Rg)$ cluster ion dissociating into $NO^-$ and Rg was estimated by subtracting the electron binding energy of the origin peak (labeled as 0,0) in the free $NO^-$ spectrum from the electron binding energy of the origin peak in a given $NO^-(Rg)$ spectrum. For the argon, krypton, and xenon complexes, these values were found to be 0.058 eV, 0.099 eV, and 0.161 eV, respectively. The ion-atom interaction energy clearly increases with the size and polarizability of the rare gas solvent. When these shifts are plotted against the polarizabilities of the rare gas atoms, they reveal a linear relationship, suggesting that weak ion-induced dipole interactions dominate the bonding in these systems.

### 3.5 $NO^-(N_2O)_{n=1-5}$

In this same family of solvated nitric oxide anions, we have also recorded the photoelectron spectra of $NO^-(N_2O)_{n=1-5}$, and these are presented in Figure 10 (ref. 55). As in the $NO^-(Rg)$ study, each of these spectra is interpreted in terms of a largely intact $NO^-$ sub-ion which is solvated and stabilized by its neutral solvent molecules. All of these $NO^-(N_2O)_n$ cluster ion spectra exhibit highly structured spectral patterns, strongly resembling those of free $NO^-$. As in previous examples, however, the individual peaks are progressively broadened, and the spectral envelopes are shifted to successively higher electron binding energies with increasing degrees of solvation. The extent of broadening and the amounts of the shifts are greater in these spectra than in the $NO^-(Rg)$ cases, indicating a substantially stronger interaction between the nitric oxide sub-anion and its nitrous oxide solvents. We presume that, while the bonding in $NO^-(Rg)$ complexes is dominated by ion-induced dipole interactions, the bonding in $NO^-(N_2O)_n$ complexes is due to ion-dipole and perhaps higher order electrostatic interactions.

The strengths of the interactions in these complexes are reflected through their ion-solvent



dissociation energies and their electron affinities. Often, in thermochemical studies, one finds that the first few ion-solvent dissociation (solvation) energies decrease rapidly with increasing cluster ion size, and this has been attributed to a partial charge transfer between the sub-ion and its neutral ligands (ref. 3). While this effect is most noticeable in the first one or two association steps, the step-wise solvation energy often continues to decrease at a slower pace for higher solvation numbers due to the weaker interaction between additional solvents and the already solvated ion. In a similar manner, electron affinities usually increase as the number of solvent molecules within the cluster increases. An initial rapid increase is again attributed to strong interactions between the ion and the

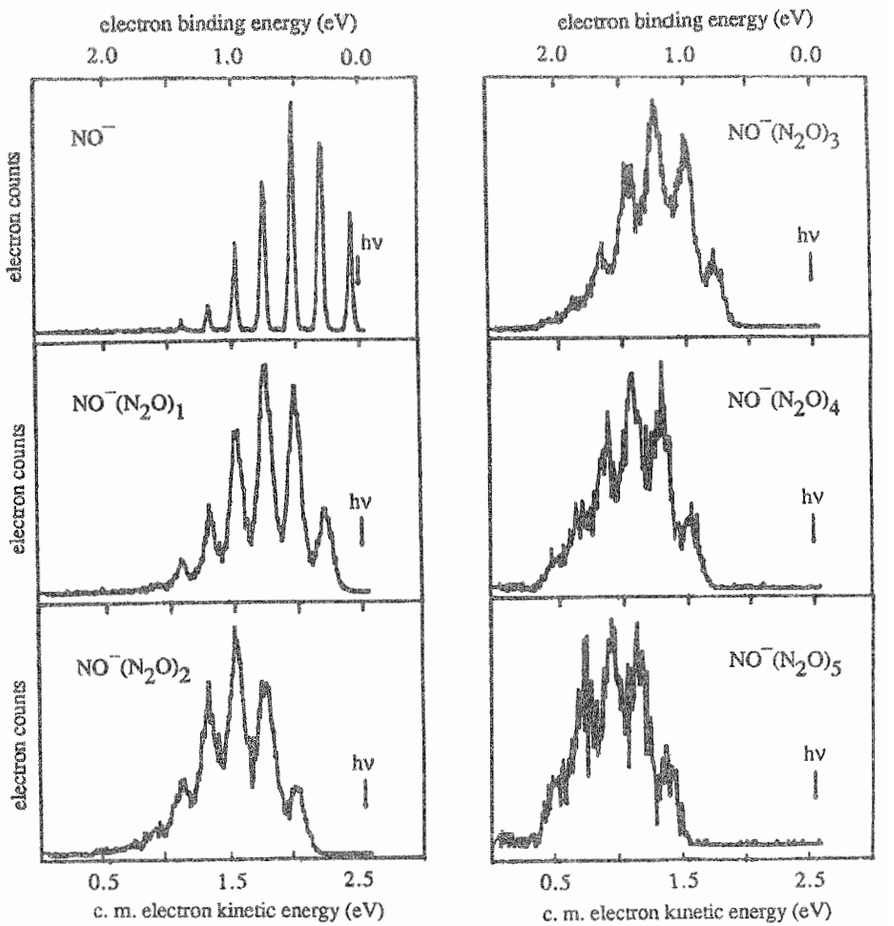


Figure 10. Photoelectron spectra of $NO^-$ and $NO^-(N_2O)_{n=1-5}$

first several solvent molecules. At some point, however, the average number of solvent molecules interacting with the anion becomes constant, causing the electron affinity to become independent of cluster size.

The electron affinities and the ion-single solvent dissociation energies for the $NO^-(N_2O)_{n=1-5}$ cluster ion series were determined from shifts of their origin peaks as previously described. In contrast to the trends depicted above, however, the ion-single solvent dissociation energies in this system were all ~0.2 eV, exhibiting no apparent decrease with cluster size. As a consequence, the electron affinities increased linearly with cluster size up through the highest cluster ion size studied with no rapid initial increase. The fact that we observe no decrease with size in ion-single solvent dissociation energies suggests that charge transfer-like effects are minimal in this system. Partial charge transfer between the sub-ion and the neutral $N_2O$ molecules may be inhibited by the large geometry change involved in attaching an electron to a $N_2O$ molecule.

In spite of this, however, some small degree of charge transfer (or charge distortion) must be occurring in these ion-molecule systems, and we were able to gauge its extent by performing a Franck-Condon analysis on the $NO^-(N_2O)_1$ spectrum (ref. 55). For this purpose, the $NO^-(N_2O)_1$ spectrum was viewed as that of a perturbed $NO^-$ ion, and special care was taken to calibrate the electron transmission function of the electron energy analyzer during this set of experiments. Our results indicated a slight contraction in the bond length of the $NO^-$ sub-ion compared to that of free $NO^-$. In principle, if the excess electron on the $NO^-$ sub-ion had been completely transferred to the $N_2O$ solvent molecule (or distorted away in some other sense), then its bond length would have contracted back to become equal to that of neutral NO. We found the $NO^-$ sub-ion bond length contraction to be ~5% of this possible contraction, thereby providing a rough measure of the extent of complexation-induced distortion of the sub-ion. Thus, while ion-solvent dissociation energy trends indicate rather weak charge transfer-like interactions in this system, the bond length contraction approach provides a more detailed picture of how much excess charge distortion actually occurs.

A final note concerns the filling of solvation shells. One might expect that shell closings would be accompanied by a dramatic change in the value of the ion-solvent dissociation energy or in the electron affinity. In this study no such change has been observed, suggesting that the first solvation shell of the nitric oxide anion contains as least five nitrous oxide molecules.



## 3.6 $NO^-(H_2O)_{n=1,2}$

Carrying our investigations of solvated nitric oxide anions still further, we have also recorded the photoelectron spectra of $NO^-(H_2O)_{n=1,2}$ and its deuterated analogs. In these systems the photoelectron spectra were essentially unstructured, the individual vibrational features of the $NO^-$ spectral pattern no longer being resolved. The shape and width of the $NO^-$ spectral envelopes, however, were faithfully retained. They were just shifted to progressively higher electron binding energies as the degree of solvation increased. Using the energy shifts between the spectral patterns in the $NO^-$, $NO^-(H_2O)_1$, and $NO^-(H_2O)_2$ spectra, the dissociation energy of $NO^-(H_2O)_1$ dissociating into $NO^-$ and $H_2O$ was determined to be ~0.75 eV, and the dissociation energy of $NO^-(H_2O)_2$ losing a single water molecule was found to be ~0.55 eV. These are among the largest solvation energies we have encountered thus far, and they doubtlessly arise due to a combination of both hydrogen bonding and electrostatic interactions between the $NO^-$ sub-ion and its water solvent molecule(s). Also, in contrast to the previously discussed system, here a substantial decrease in the solvation energies is observed between the first and the second solvation steps. Presumably, the sub-ion can hydrogen bond more strongly to one neutral water molecule (possibly involving partial charge transfer effects) than to two, so the strength of the interaction decreases as the number of solvent molecules around the sub-ion increases.

Taken together, these studies of solvated nitric oxide anions illustrate the range of interactions involved in the bonding of ion-molecule complexes. The cluster ions, $NO^-(Ar)$, $NO^-(Kr)$, and $NO^-(Xe)$, are bound by weak ion-induced dipole interactions, and their ion-atom dissociation energies lie in the range, 60-160 meV. In the case of the $NO^-(N_2O)_n$ systems, ion-dipole and ion-quadrupole interactions probably dominate the bonding, their dissociation energies being ~200 meV, considerably larger than the anion-rare gas dissociation energies. Lastly, the $NO^-(H_2O)_{n=1,2}$ study provides examples of ion-molecule complexes which exhibit still stronger interactions, probably due to hydrogen bonding and electrostatic interactions together. For these systems, ion-molecule dissociation energies on the order of 500-700 meV were observed, about three times that of the nitrous oxide cluster ion dissociation energies and almost ten times that of the rare gas ion complexes.

### 3.7 $O_2^-(N_2)$

Using pulsed negative ion photoelectron spectroscopy, Johnson and his coworkers have also contributed substantially to the study of anion-molecule complexes. Of particular interest is a pair of complexes containing $O_2^-$ sub-ions, one solvated by nitrogen and the other by oxygen. The ion-molecule complex, $O_2^-(N_2)$, was one of several $N_2O_2^-$ isomers investigated by Johnson (ref. 29), and its photoelectron spectrum is presented in Figure 11 along with the spectrum of $O_2^-$. As in all the ion-molecule complexes previously surveyed, the main features in this spectrum are similar to the features of the free sub-ion except for being broadened and shifted to higher electron binding energy.

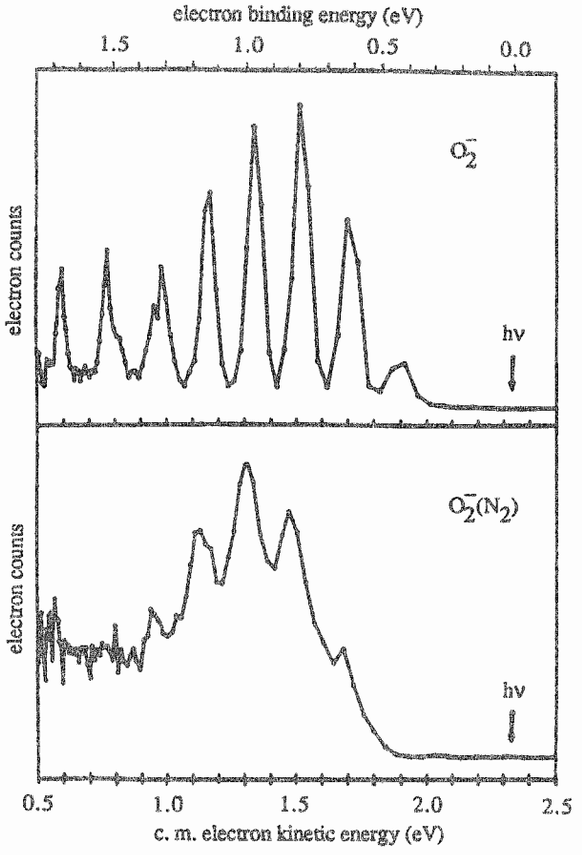


Figure 11. Photoelectron spectra $O_2^-$ and $O_2^-(N_2)$



The vibrational peak spacing in the ion-molecule spectrum is 0.19 eV, similar to that of $O_2$, (0.187 eV). The vibrational spacing of NO, on the other hand, is somewhat larger (0.226 eV), indicating that the sub-ion from which the electron was photodetached was $O_2^-$ rather than $NO^-$. For this particular isomer of $N_2O_2^-$, the ion-molecule complex was thus interpreted to be $O_2^-(N_2)$ rather than $NO^-(NO)$. The electron affinity of the $O_2(N_2)$ cluster was determined in the usual way and was found to be ~0.69 eV. In addition, the ion-neutral bond dissociation energy for $O_2^-(N_2)$ was determined from origin shifts to be ~0.26 eV.

### 3.8 $O_2^-(O_2)$

The main spectral feature in the $O_4^-$ photoelectron spectrum is a single broad peak with no recognizable vibrational structure (see Figure 12). Johnson and his colleagues (ref. 28) provide two arguments for interpreting their $O_4^-$ spectrum as that of $O_2^-(O_2)$. First, the width of the main feature corresponds to the width of the vibrational envelope for the main electronic band in the photoelectron spectrum of free $O_2^-$. Second, this broad peak has an onset that is about ~0.6 eV higher in electron binding energy than the origin of the free $O_2^-$ spectrum, and such a shift is in agreement with thermochemical measurements for the ion-molecule dissociation energy of $O_4^-$ (0.59 eV).

The spectrum also contains a series of low intensity peaks to the high electron kinetic energy side of the main spectral feature. These features exhibit a non-linear laser-power dependence, implying that they arise due to a multiphoton process. They also occur at the same energies as do the main features of the free $O_2^-$ spectrum, and they are each separated by an energy which is close to the $O_2$ vibrational spacing observed in the $O_2^-$ spectrum. These peaks are therefore attributed to a two photon process in which $O_4^-$ is first photodissociated into $O_2^-$ and most probably $O_2$, followed by the photodetachment of the nascent $O_2^-$.

### 3.9 $(ROHF)^-$

Important contributions to our understanding of anion-molecule complexes have also come from photodetachment experiments performed in an ion cyclotron resonance spectrometer. In this photodetachment technique a tunable-frequency, rather than a fixed-frequency, laser is utilized, and the amount of photodetachment is measured as a function of photon energy. Brauman and his

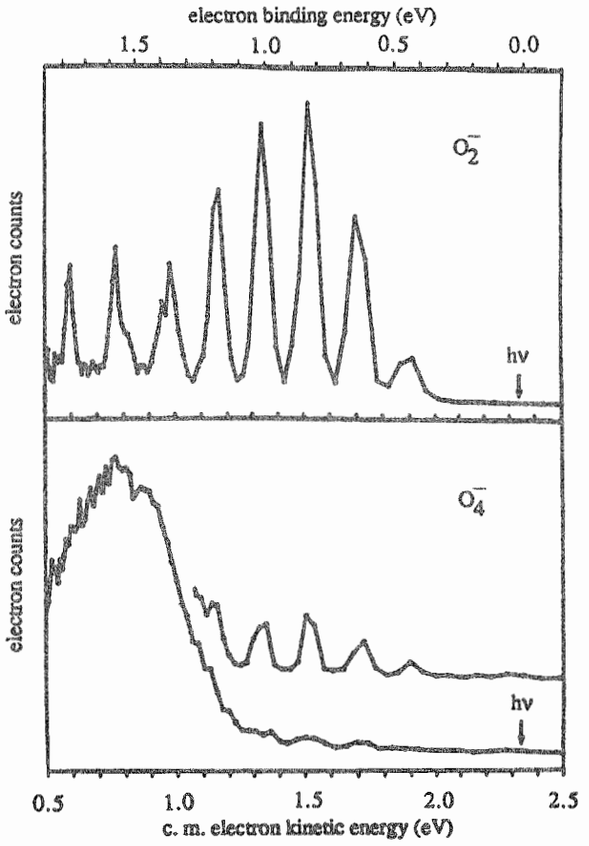


Figure 12. Photoelectron spectra of $O_2^-$ and $O_4^-$. The upper spectral trace in the $O_4^-$ spectrum was obtained at 10 times higher laser power.

coworkers (ref. 40-42) have used this approach to study a series of ion-molecule complexes of the form $(ROHF)^-$, where R represents an organic group. These complexes represent intermediate species in gas-phase proton transfer reactions between alcohols and fluoride anions. On energetic grounds alone, it is difficult to predict whether $(ROHF)^-$ would be present as $F^-(ROH)$ or as $RO^-(HF)$. These two species can, however, be distinguished through photodetachment experiments. While the photodetachment threshold energy (the electron binding energy of its origin) of $F^-(ROH)$ lies outside of the range of photon energies that was available in this experiment, the threshold energy for $RO^-(HF)$ is roughly predictable and was accessible to the experiment. Brauman and his colleagues studied $(ROHF)^-$ systems in which the R's were methyl, ethyl,



isopropyl, tertbutyl, neopentyl, and benzyl groups. Of these, photodetachment signals were observed only in $(C_6H_5CH_2OHF)^-$. The threshold energy for this ion was 3.05 eV, implying that it is $C_6H_5CH_2O^-(HF)$ rather than $F^-(C_6H_5CH_2OH)$. This value was used in an appropriate thermochemical cycle to determine an ion-molecule dissociation (solvation) energy of 1.26 eV, which is a reasonable number for hydrogen bonded ion-molecule complexes. The other five solvated anions studied did not photodetach within this energy range, indicating they are probably of the form $F^-(ROH)$. These results were rationalized in terms of relative gas-phase acidities.

## 4. MOLECULAR CLUSTER ANIONS EXHIBITING EXCESS CHARGE DELOCALIZATION

Unlike anion-molecule complexes where the excess negative charge is highly localized, there are other molecular cluster anions in which the excess charge is delocalized over all or part of the cluster ion. Excess charge dispersal in negative cluster ions can appear in a variety of ways, and each of these can vary substantially in degree. In some systems, negative charge delocalization may manifest itself as electron tunneling or "hopping" between energetically and structurally equivalent sites within the cluster ion, while in others its contributions to bonding may arise in the sense of covalency in ion-neutral bonds. In some systems, such as $(SO_2)_2^-$ (ref. 10) and possibly in $(CO_2)_2^-$ and $(O_2)_2^-$, the molecular components of the dimer may resonantly share the excess electron, while in $(H_2O)_2^-$ the excess electron is most likely bound by the dipole field of the neutral water dimer. In larger cluster anions, still other forms of electron delocalization may occur. In $(H_2O)_n^-$ and $(NH_3)_n^-$, systems comprised of molecules which can not separately bind electrons, there may be some cluster size regimes where the excess electron resides in a delocalized surface state, while for other sizes it exists as an internal state, either in a cavity where it interacts with several solvent molecules or perhaps delocalized throughout the entire cluster ion. Manifestations of charge delocalization are also seen in anionic systems which are cousins to cluster anions. In $(ClHCl)^-$, which has been photodetached by Neumark and coworkers (ref. 32), the anion may be roughly envisioned as a proton oscillating between two chlorine negative ions, ie. the excess negative charge being delocalized (albeit slightly asymmetrically) to the chlorine ends of this linear system. And, in the case of the tetrahedral isomer of $NH_4^-$, the anion is most probably comprised of an ammonium cation

core with two highly delocalized (Rydberg-like) electrons trapped in its field (ref. 59). While this section of our chapter focuses on excess charge dispersal in molecular cluster anions and related systems, we should also mention, before proceeding, the enormous importance of excess charge delocalization in atomic cluster anions, which are, with only a few exceptions (such as $Xe_n^-$), metal and semimetal cluster anions. The subject of metal cluster anions is addressed in section five of this chapter and in the companion chapter by R. E. Smalley and his colleagues. In this section, we exemplify molecular cluster anions exhibiting substantial excess charge delocalization by presenting some of our results on the photodetachment of water cluster anions.

### 4.1 Water Cluster Anions

As mentioned above, an individual water molecule is not thought to be able to bind an excess electron. Nevertheless, bulk water, and several other fluids comprised of molecules with non-positive adiabatic electron affinities, are able to accommodate excess electrons. With this in mind, it has often been suggested over the years that $(H_2O)_n^-$ cluster ions ought to exist, and that they might be the gas-phase counterparts to condensed-phase solvated (hydrated) electrons. A few years ago, these long-predicted entities were observed for the first time in the gas phase by Haberland (ref. 64). Following these developments, we generated water cluster anions from neat water expansions in a supersonic expansion ion source and recorded the photoelectron spectra of $(H_2O)_{n=11\text{-}15,19}^-$ (ref. 77). More recently, we collaborated with the Haberland group to record the photoelectron spectra of still more water cluster anions, and in these experiments we utilized argon/water expansions (ref. 78). The list of water cluster anions that we have photodetached thus far includes: $(H_2O)_{n=2,6,7,10\text{-}25,30,34,37,40}^-$, $(D_2O)_{n=2,6,7,11\text{-}23}^-$, $Ar(H_2O)_{n=2,6,7}^-$, $Ar(D_2O)_{n=2,6,7}^-$, and $Ar_2(D_2O)_6^-$.

The formation of various sizes of water cluster anions is particularly sensitive to ion source conditions. Figure 13 shows the various families of water cluster anions that were generated in our supersonic expansion ion source under three different sets of source conditions. Observations such as these led Haberland, who had earlier seen essentially the same mass spectra under comparable source conditions, to suggest that there probably exist at least three different classes of water cluster anions. At very low concentrations of water, one sees only the water dimer anion and its argon



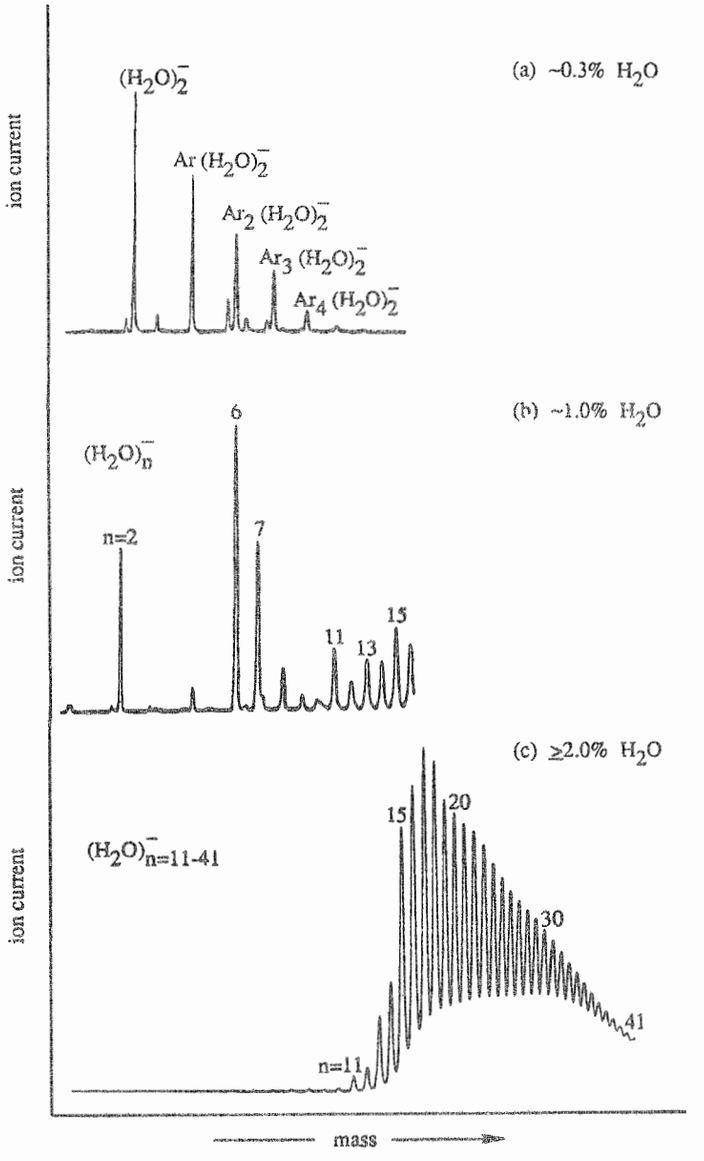


Figure 13. Mass spectra of water cluster anions generated under varying source conditions. The anions were produced by coexpanding the indicated percentage of water vapor with argon.

clusters. As the water concentration is increased, new species such as $(H_2O)_6^-$ and $(H_2O)_7^-$ appear, and these behave similarly to one another with source conditions yet differently than $(H_2O)_2^-$. At still higher water concentrations, the larger water cluster anions, starting with $(H_2O)_{11}^-$, have grown to dominate the mass spectrum, and the smaller cluster anions have essentially disappeared. This section of the chapter is organized in terms of these three families of water cluster anions with $(H_2O)_2^-$ being discussed first, $(H_2O)_{n=6,7}^-$ being presented next, and with the larger cluster ions. $(H_2O)_{n\geq 11}^-$ being discussed last. The water dimer anion photoelectron spectra are shown in Figure 14, the spectra for $(H_2O)_{n=6,7}^-$ and $(D_2O)_{n=6,7}^-$ are presented in Figure 15, and the spectra of $(H_2O)_{n=11\text{-}25,30,34,37,40}^-$ are shown in Figure 16.

The water dimer anion has been depicted as a dipole bound negative ion. Calculations by Berne et al. and by Landman, Jortner, and coworkers (ref. 79,80) have predicted the electron affinity of water dimer to be very small (~3-6 meV), and the structure of $(H_2O)_2^-$ to be the same as that of the neutral water dimer, $(H_2O)_2$. In this picture, the attachment of an electron to the neutral dimer is expected to be only a slight perturbation on the system. The photoelectron spectrum of the water dimer anion exhibits one large peak and two smaller peaks to the high electron binding energy side of the main peak. We assign the main feature as the origin-containing peak. The electron binding energy of the center of this feature is ~34 meV, and this is the vertical detachment energy for the water dimer anion. The two smaller peaks are separated from the main peak by energies corresponding to a $H_2O$ bend and stretch, respectively. While the position of the main peak in the photoelectron spectrum of $(D_2O)_2^-$ does not change relative to that in the $(H_2O)_2^-$ spectrum, the energy spacings between the main peak and its two smaller peaks correspond to those of a $D_2O$ bend and stretch, respectively. This implies that water stretches and bends are excited during photodetachment, and that there is a structural difference between the dimer anion and the dimer neutral, ie. the addition of an excess electron to the neutral water dimer distorts at least part of its structure. The low intensity of the two smaller peaks, on the other hand, suggests that the distortion is rather slight. Since the structural difference between the anion and its corresponding neutral is small, the adiabatic electron affinity of water dimer is probably only a little less than 34 meV, the vertical detachment energy. Thus, the calculations on water dimer anion and the experimental results appear to be in qualitative accord, with both the energetic and the structural implications of the experiment suggesting that the strength of the electron-dimer interaction is a little stronger than that



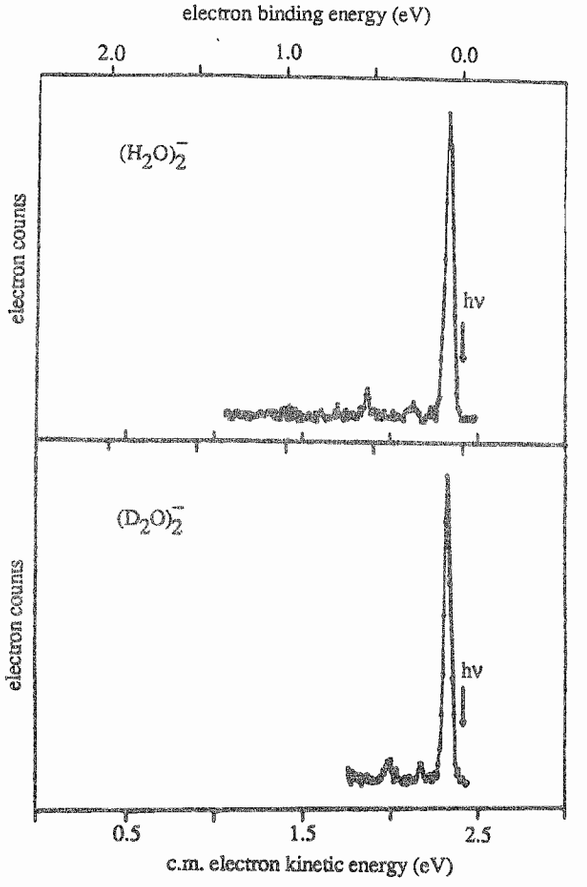


Figure 14. The photoelectron spectra of $(H_2O)_2^-$ and $(D_2O)_2^-$

expected on the basis of calculations.

Since the photoelectron spectra of water hexamer anion and water heptamer anion are rather similar, we will consider only the water hexamer anion here. Three peaks appear in the $(H_2O)_6^-$ spectrum, a large peak and two smaller peaks, one of which appears on the high electron binding energy side of the main peak and the other which occurs on its low binding energy side. While the energy spacing between the largest peak and the highest electron binding energy peak is very close to the energy of a $H_2O$ stretching frequency, the spacing between the main feature and the lowest

binding energy feature does not correspond to either a water stretch or a water bend. Also, while the two lowest electron binding energy peaks in the $(D_2O)_6^-$ spectrum do not shift significantly upon deuteration, the spacing between the middle (the largest intensity) peak and the highest binding energy feature in the deuterated spectrum contracts (relative to its value in the $(H_2O)_6^-$ spectrum) to an energy corresponding to a $D_2O$ stretching frequency. This may mean that the two lowest binding

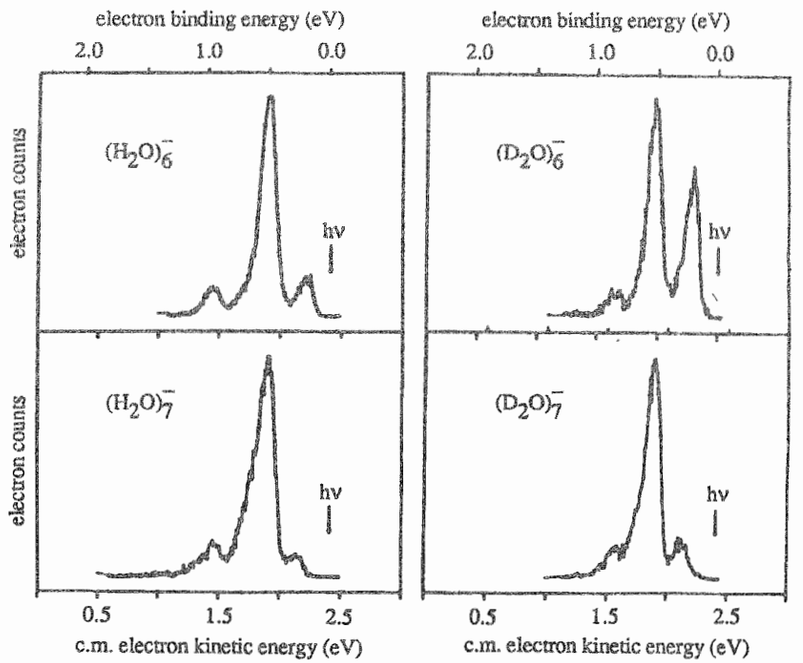


Figure 15. The photoelectron spectra of $(H_2O)^-_{n=6,7}$ and $(D_2O)^-_{n=6,7}$

energy peaks in the water hexamer anion photoelectron spectra arise due to the photodetachment of two different forms of the cluster anion, and that the highest binding energy peak in these spectra is due to the excitation of a water stretch during the photodetachment of the higher binding energy isomer of the hexamer anion, ie. there is a significant structural difference between the higher binding energy isomer of the anion and its corresponding neutral. It is intriguing to wonder if the low binding energy isomer of the anion could be a surface electron state, while the higher binding energy isomer might correspond to an internal electron state.



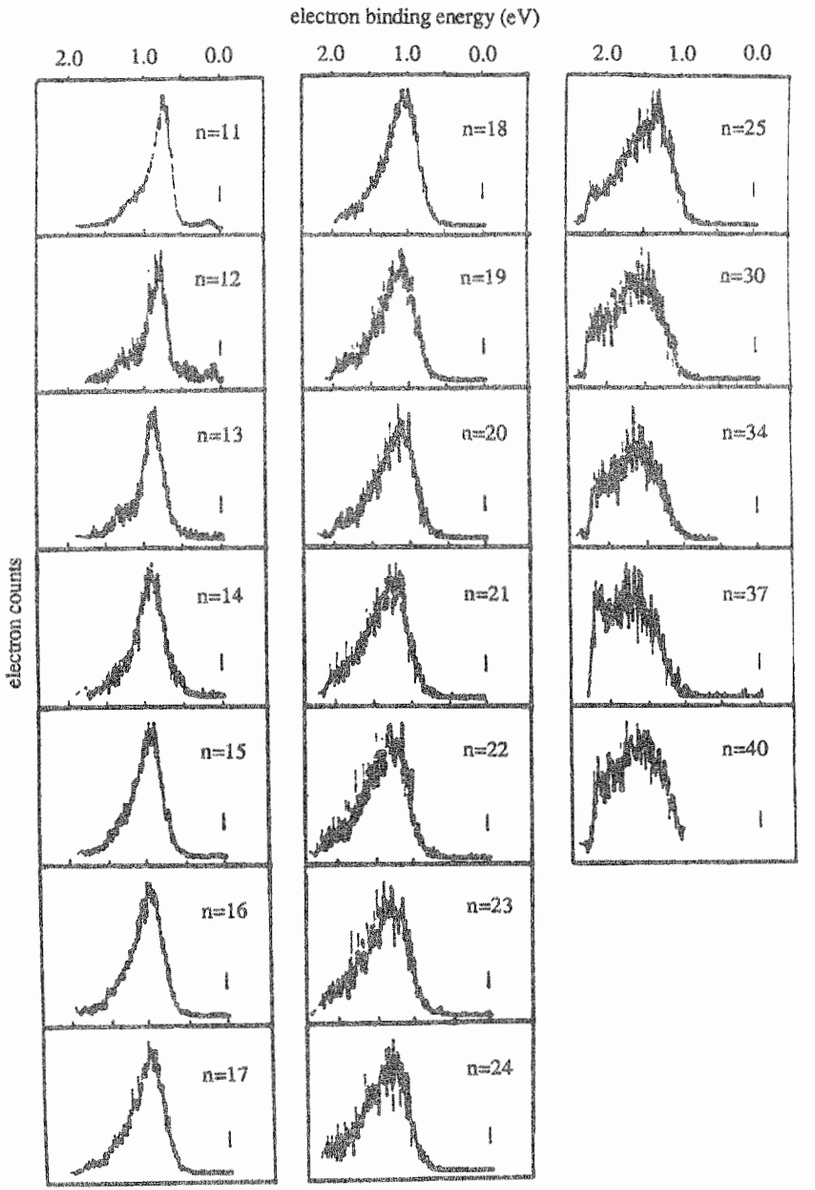


Figure 16. The photoelectron spectra of $(H_2O)^-_{n=11\text{-}25,30,34,37,40}$

Essentially, the photoelectron spectra of the larger (n≥11) water cluster anions consist of single broadened peaks which are shifted to successively higher electron binding energies (and progressively broadened) with increasing cluster ion size (see Figure 16). The electron binding energies of the fitted peak maxima of these spectra correspond to the vertical detachment energies of their cluster anions. A plot of these vertical detachment energies (VDE) vs. cluster size (n) shows that the available VDE values vary smoothly from ~0.75 eV for n=11 to ~1.7 eV for n=40. An important, but as yet unresolved issue having to do with electron delocalization in water cluster anions involves the existence of surface versus internal electron states in these systems. Presumably, hydrated electrons in the condensed phase are internal electron states, while surface electron states should probably be viewed as precursors to hydrated electron-like states. Based on the results of their recent calculations, Landman, Jortner, and their colleagues (ref. 15,81) concluded that the water cluster anions we have studied thus far are surface electron states. Their calculations find that the transition from surface electron states to internal electron states should occur somewhere between n=32 and n=64. Our photoelectron data do not permit us to conclusively distinguish between surface and internal states. On the other hand, one might expect a discontinuity in the variation of VDE vs. n at the cluster ion size where the transition from surface to internal states takes place. Thus far, we have measured VDE's of water cluster anions up to n=40, and we see only a smooth variation with cluster size with no obvious discontinuities. Clearly, the partnership between theory and experiment is essential to progress on this intriguing topic.

## 5. METAL CLUSTER ANIONS

While the negatively charged cluster anions discussed previously consisted primarily of molecular components, the metal cluster anions to be considered in this section are comprised of atoms. Particularly important in the study of metals and metal cluster anions is a consideration of their electronic properties. Often, properties such as the ionization potentials and electron affinities of metals vary in magnitude over several electron volts from their atomic to their bulk values, and clusters and aggregates of intermediate size have electronic properties with intermediate values. As an example, consider sodium, where the ionization potential decreases gradually from its atomic value of 5.139 eV to its bulk (work function) value of 2.28 eV. Likewise, the electron affinity of



sodium increases by a comparable amount from its atomic value of 0.548 eV to the bulk work function. Changes of this magnitude in going from the atomic to the bulk state are exhibited by many metals, and these are probably of substantial chemical significance. In fact, for phenomena occurring in the regime of very small sizes, the pertinent value of a given electronic property may be neither its atomic nor its bulk value but something intermediate.

The photoelectron spectra of metal cluster anions provide important information about the electronic properties of their corresponding neutral clusters. In the spectrum of a particular metal cluster anion, bands arise due to photodetachment transitions between the ground state of the anion and the ground and various low lying electronic states of the corresponding neutral (at the geometry of the negative ion). Thus, low lying electronic state splittings for neutral metal clusters are obtained, including splittings between optically dark electronic states. Equally important, adiabatic electron affinities can be determined from the transition between the ground electronic and vibrational states of the anion and the neutral. Studying an entire series of metal clusters using negative ion photoelectron spectroscopy allows one to map out the variation in electron affinities and low lying electronic state structure as a function of cluster size, tracing the evolution of these electronic properties from their atomic values toward the values of the macroscopic bulk state.

The photodetachment of metal cluster anions has been investigated by both pulsed and continuous beam photoelectron techniques. Systems which have been studied by Smalley and by Meiwes-Broer with the pulsed technique are covered more thoroughly in this volume in the chapter by Smalley, et al.. This section of our chapter surveys selected examples of metal cluster anions investigated by continuous beam negative ion photoelectron spectroscopy. In particular, Lineberger and coworkers have studied a number of transition metal dimer and trimer anions, using them to probe the nature and extent of *d* orbital interactions in transition metal bonding. In addition, they have also studied several transition metal cluster anion series, including $Cu^-_{n=2-10}$, $Ag^-_{n=2-6}$, and $Ni^-_{n=2-8}$. In our laboratory, we have used this technique to investigate the periodic trends in the electronic properties of the alkali metal cluster anions, $Na^-_{n=2-5}$, $K^-_{n=2-7}$, $Rb^-_{n=2,3}$ $Cs^-_{n=2,3}$, $NaK^-$, $KRb^-$, $KCs^-$, and $RbCs^-$. Alkali metals differ from most transition metals in that their *d* orbitals do not participate significantly in interatomic interactions. Since alkali atoms have hydrogen-like electronic structures, the alkali metals are the simplest and therefore the most theoretically-tractable of metals. Below, both the transition metal and alkali metal systems are

highlighted. For each system, metal dimers and trimers are examined first because of their value in illuminating the initial interactions among metal atoms, and then, trends in an individual metal cluster series are explored.

### 5.1 Transition Metal Dimers and Trimers

The relative contributions of *s* and *d* orbitals to the bonding of transition metal dimers and trimers has been a subject of considerable interest (ref. 82), and these contributions can be understood in terms of the periodic behavior of their atoms. In the more massive atoms of a given transition metal row, the bonding is expected to be increasingly dominated by *s* orbitals, with weaker interactions among the *d* orbitals resulting in their decreasing contribution to bonding. On the other hand, the more massive atoms of a particular transition metal column (group) display stronger interactions among the *d* orbitals. Thus, in a given column *d* orbital bonding is expected to become more significant in the second and third row metals than in their first row counterparts.

Recently, Leopold and Lineberger have recorded the photoelectron spectra of $Fe_2^-$ and $Co_2^-$ (ref. 47), shown in Figure 17, and these spectra shed considerable light on the subject of transition metal bonding. Four experimental facts were derived from these spectra. (1) The $Fe_2^-$ spectrum exhibits transitions to two vibronic band systems of $Fe_2$, while the spectrum of $Co_2^-$ contains transitions to three or more such vibronic band systems. (2) The bond lengths and vibrational frequencies of the ground state and first excited state of the neutral are essentially the same. (3) The anion has a longer bond length and lower vibrational frequency than its corresponding neutral. (4) Despite this, the anion has a dissociation energy which is substantially larger than that of its neutral.

Leopold, Lineberger, and their colleagues have presented an interpretation for $Fe_2^-$ explaining these observations (ref. 49), and an analogous interpretation can be applied to $Co_2^-$. These authors envision a neutral dimer ground state which arises from the mixing of a $4s^2 3d^6$ Fe atomic ground state and a $4s^1 3d^7$ Fe atomic excited state. This produces a neutral $Fe_2$ dimer with a $(4s\sigma)^2(4s\sigma^*)^1(3d)^{13}$ ground state and an anion with a $(4s\sigma)^2(4s\sigma^*)^2(3d)^{13}$ ground state, and electron detachment is believed to occur from the mildly antibonding $4s\sigma^*$ orbital of the anion. The two vibronic progressions observed in the $Fe_2^-$ spectrum arise from transitions between the ground state of the anion and the ground and first excited states of the neutral. These two neutral states are



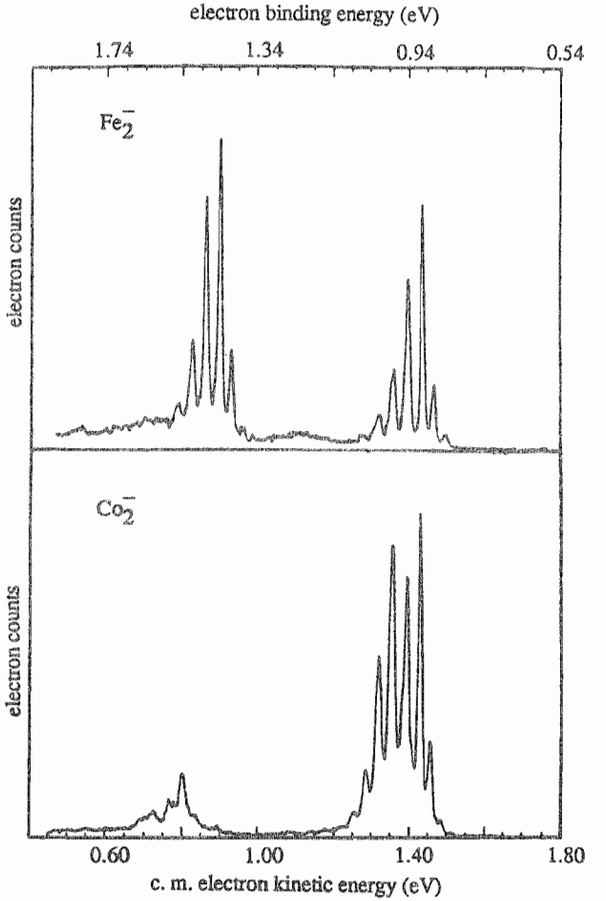


Figure 17. The photoelectron spectra of $Fe_2^-$ and $Co_2^-$

similar in that they have identical $\sigma^*$ and $\sigma$ occupations, but they differ in terms of the spin coupling between the $(4s\sigma^*)^1$ electron and the $(3d)^{13}$ "core". The similar bond lengths and vibrational frequencies of the ground and first excited states of the neutral are explained in terms of the identical $\sigma^*$ and $\sigma$ occupations. The formation of the anion results from the addition of an electron to a $4s\sigma^*$ orbital, and this accounts for the longer bond length and lower vibrational frequency of the anion relative to the neutral. In order to rationalize the larger bond dissociation energy of the anion relative to the neutral, Leopold et al. note that the dimer anion can be formed from ground state atomic orbitals, while the dimer neutral is formed from the mixing of ground and excited state atomic

orbitals. Under this interpretation, formation of the neutral dimer requires a 4*s* electron to be promoted into the 3*d* orbitals. Thus, the bonding molecular orbital of the neutral is of higher energy than that of the dimer anion, leading to a greater dissociation energy for the anion. The appearance of only a few low lying electronic states in the photoelectron spectra of $Fe_2^-$ and $Co_2^-$ is in contrast with recent ab initio calculations (ref. 83,84) which predicted both $Fe_2$ and $Co_2$ to have a large number of low lying electronic states due to weakly interacting *d* orbitals. This dearth of low lying electronic states led Lineberger et al. to suggest that the bonding interactions of the *d* orbitals in these dimers are stronger than had been supposed, and that this results in significant state splittings and therefore in fewer low lying states. In addition, a comparison of the bond length and vibrational frequency of $Fe_2$ with values for transition metal dimers containing single 4*s*-4*s* bonds supported their contention that 3*d*-3*d* bonding is important in $Fe_2$.

Moving on from iron and cobalt to more massive first row transition metals, the next metal with an available dimer anion spectrum is copper. Copper dimer should exhibit bonding characteristics consistent with a primarily 4*s*σ bonded species. Since copper's *d* orbitals are completely filled, they are not expected to participate significantly in bonding. On the other hand, the filled *d* orbitals also preclude a high density of low lying electronic states otherwise expected in a molecule with weakly interacting *d* orbitals. The photoelectron spectrum of $Cu_2^-$, recorded by Leopold, Ho, and Lineberger (ref. 48) and shown in Figure 18, is consistent with this picture. The spectrum exhibits a lone vibronic progression corresponding to transitions between the ground electronic state of the dimer anion and the ground electronic state of the neutral dimer. As expected, no dense manifold of excited electronic states is observed. The picture of $Cu_2$ bonding presented above implies that the additional electron in $Cu_2^-$ occupies a 4*s*σ* antibonding orbital. In accord with this expectation, the photoelectron spectrum of $Cu_2^-$ reveals an anion with a longer bond length and a lower vibrational frequency than its neutral. The bond lengths of $Cu_2$ and $Cu_2^-$ are 2.2197 Å and 2.345 Å, respectively, while the $Cu_2$ vibrational frequency is 265 $cm^{-1}$ and that of $Cu_2^-$ is 210 $cm^{-1}$. The adiabatic electron affinity of $Cu_2$, determined from the $Cu_2^-$ spectrum, is 0.842 eV. Using this value in a thermochemical cycle, the anion dissociation energy was found to be 1.57 eV, approximately 20% less than neutral $Cu_2$.

As mentioned earlier, in the heavier atoms of a particular transition metal row, interactions among the *d* orbitals decrease, while the vertical trend in a transition metal column displays



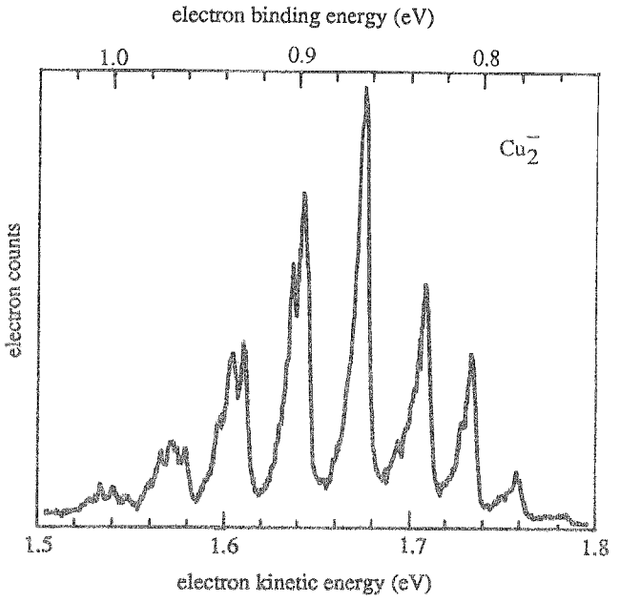


Figure 18. The photoelectron spectrum of $Cu_2^-$

increasing *d* orbital interactions with increasing mass. Thus, dimers and trimers of the second and third row transition metals exhibit more *d* orbital interactions and stronger multiple bonding than their first row counterparts. Consider for example, the group VIIA metal dimers, where the first row dimer, $Mn_2$, is a van der Waals molecule (ref. 82), even though the third row dimer $Re_2$ is thought to be strongly bound (ref. 85,86). This suggests that the *d* orbitals in $Re_2$ play an important role in bonding, and that there should exist relatively few low lying electronic states in $Re_2$. When Leopold, Miller, and Lineberger (ref. 46) recorded the photoelectron spectrum of $Re_2^-$, (see Figure 19), they saw evidence for four low lying electronic states in $Re_2$, which is consistent with this expectation. In addition, the vibrational frequencies of $Re_2^-$ (320 $cm^{-1}$) and $Re_2$ (340 $cm^{-1}$) imply large force constants in both the anion and the neutral. These are comparable to the force constants of $Mo_2$ and $V_2$, systems known to exhibit substantial multiple bonding. This suggests the occurrence of multiple bonding in both $Re_2$ and $Re_2^-$, with significant bonding contributions from the *d* orbitals.

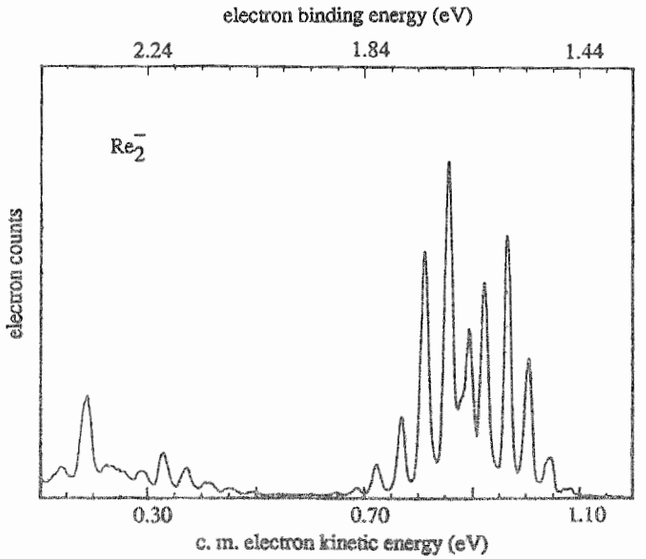


Figure 19. The photoelectron spectrum of $Re_2^-$

Evidence for the increasing role of *d* orbital electrons in the bonding of second and third row transition metals is also seen in the photoelectron spectra of the nickel group trimer anions (see Figure 20), which were recorded by Ervin, Ho, and Lineberger (ref. 50). The spectrum of $Ni_3^-$ contains diffuse bands which may arise from several overlapping electronic states. This is consistent with weakly interacting *d* orbitals producing a dense manifold of low lying electronic states. The second trimer in this column, $Pd_3^-$, has a less congested spectrum, exhibiting both broad features and resolved vibrational progressions. Lastly, the spectrum of $Pt_3^-$ exhibits sharp features and resolved progressions, reflective of a smaller number of low lying electronic states. This decreasing number of low lying states with increasingly massive elements is consistent with a growing involvement of *d* orbitals in bonding.

### 5.2 Transition Metal Cluster Series

The determination of electron affinities and electronic state splittings for an entire series of metal clusters has been the objective in several photoelectron spectroscopic studies of metal cluster anions.



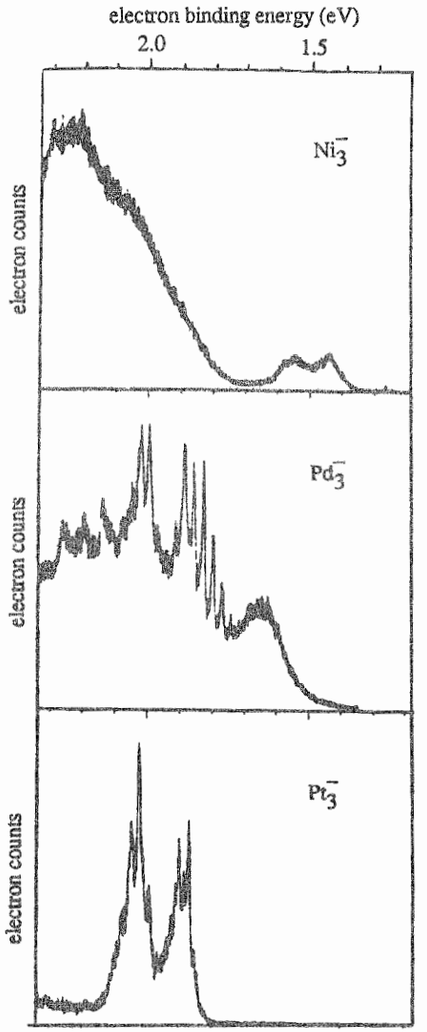


Figure 20. The photoelectron spectra of $Ni_3^-$, $Pd_3^-$, and $Pt_3^-$

Of the transition metal systems studied by negative ion photoelectron spectroscopy, copper is particularly illuminating, and it will be used here to illustrate trends in the electronic properties of metal clusters. Copper cluster anions have been studied by Lineberger et al. (ref. 48) using continuous beam photoelectron spectroscopy with visible photons, while both Smalley and Meiwes-

Broer have used pulsed ultraviolet methods to study them. Lineberger's spectra of $Cu^-_{n=1-10}$ are presented in Figure 21. These spectra provide electron affinities of all the copper clusters studied, along with the splittings between the ground and first excited electronic states in the corresponding neutrals for several of these clusters.

Two important trends are observed in regard to the copper cluster electron affinities: an overall increase in electron affinity values with increasing cluster size, and an odd-even alternation where clusters containing an odd number of atoms have higher electron affinities than adjacent-sized clusters comprised of an even number of atoms. The first trend has been modeled via the electrostatic spherical drop model, in which a metal cluster is approximated as a perfectly conducting sphere with radius proportional to $n^{1/3}$, where n is the number of metal atoms in the cluster. While the simple spherical drop model provides qualitative agreement with the observed trend, it fails to give quantitative accuracy. However, by modifying the model to include a "charge spillout factor", which is added to the calculated cluster radius, quantitative agreement can be achieved. The second trend observed among the copper cluster electron affinities is that odd numbered clusters tend to have higher electron affinities than adjacent-sized even numbered clusters. Alternations such as this have also been observed for ionization potentials of copper and alkali metals, but with even sized clusters having higher ionization potentials than neighboring odd sized clusters. To a first approximation, these trends are understandable in terms of electron pairing. While the spherical drop model predicts the correct trend for electron affinity vs. cluster size, it cannot reproduce the odd-even alternation. Other models, on the other hand, such as extended Hückel, jellium, and ab initio approaches do predict such a pattern.

The energy splittings between the ground and the first excited electronic states in a neutral cluster series provide some insight into the variation of the HOMO-LUMO energy gap as a function of cluster size. The HOMO-LUMO gap is expected to decrease as cluster sizes increase and as the cluster electronic states converge toward the band structure. Excited electronic states were observed in the spectra of several copper clusters, and lower limits were set on the electronic state splittings for others. These electronic energy level splittings were found to decrease rapidly with increasing cluster size, consistent with the expected trend. The only exception was $Cu_8$, where an unusually large lower limit was established for the first electronic state splitting. The large HOMO-LUMO gap in $Cu_8$, along with its low electron affinity implies that the electronic structure of $Cu_8$ is particularly



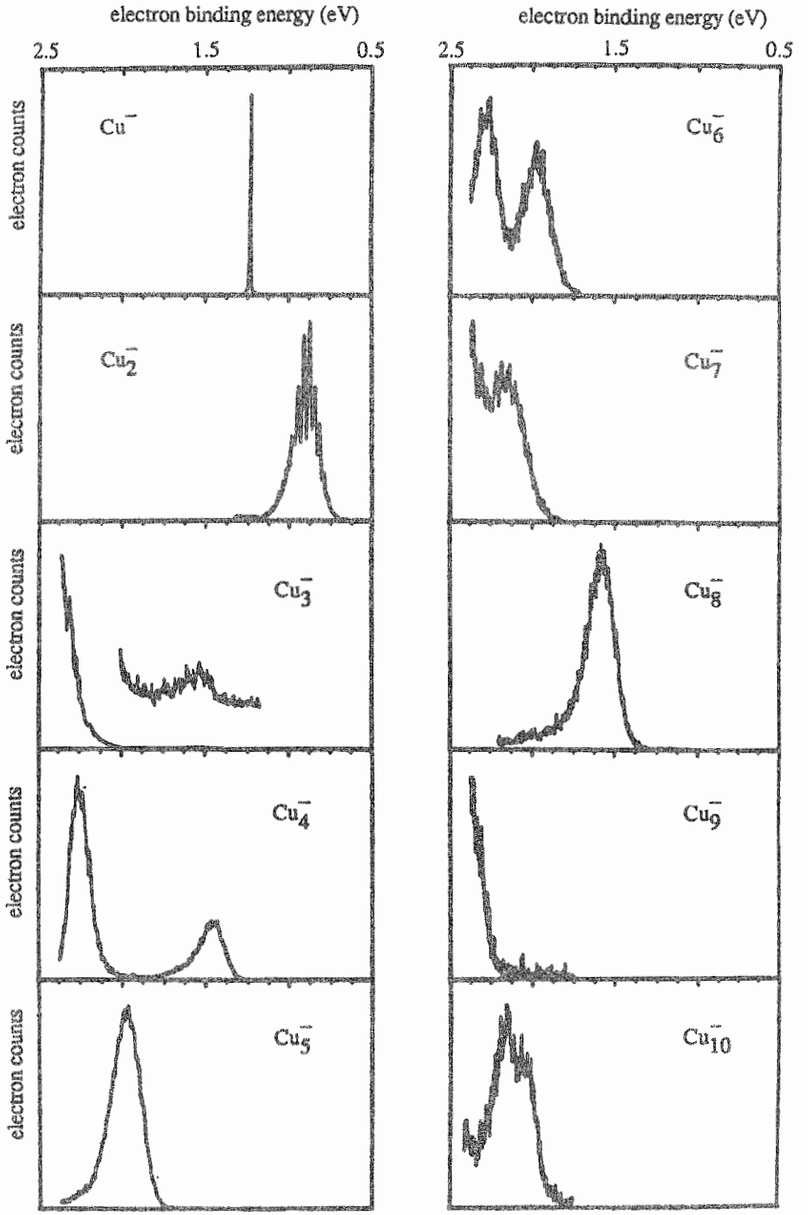


Figure 21. The photoelectron spectra of $Cu^-_{n=1-10}$

stable, consistent with the shell closing predicted for the octamers of coinage and alkali metals by electron shell models.

### 5.3 Alkali Metal Dimers and Trimers

We have recorded the photoelectron spectra of the homogeneous alkali metal dimer and trimer anions, $Na^-_{n=2,3}$, $K^-_{n=2,3}$, $Rb^-_{n=2,3}$, and $Cs^-_{n=2,3}$, which are presented in Figure 22. For comparison, this figure also includes the photoelectron spectra of the alkali metal atomic anions. In addition, we have also studied the heterogeneous alkali dimers $NaK^-$, $KRb^-$, $KCs^-$, and $RbCs^-$,

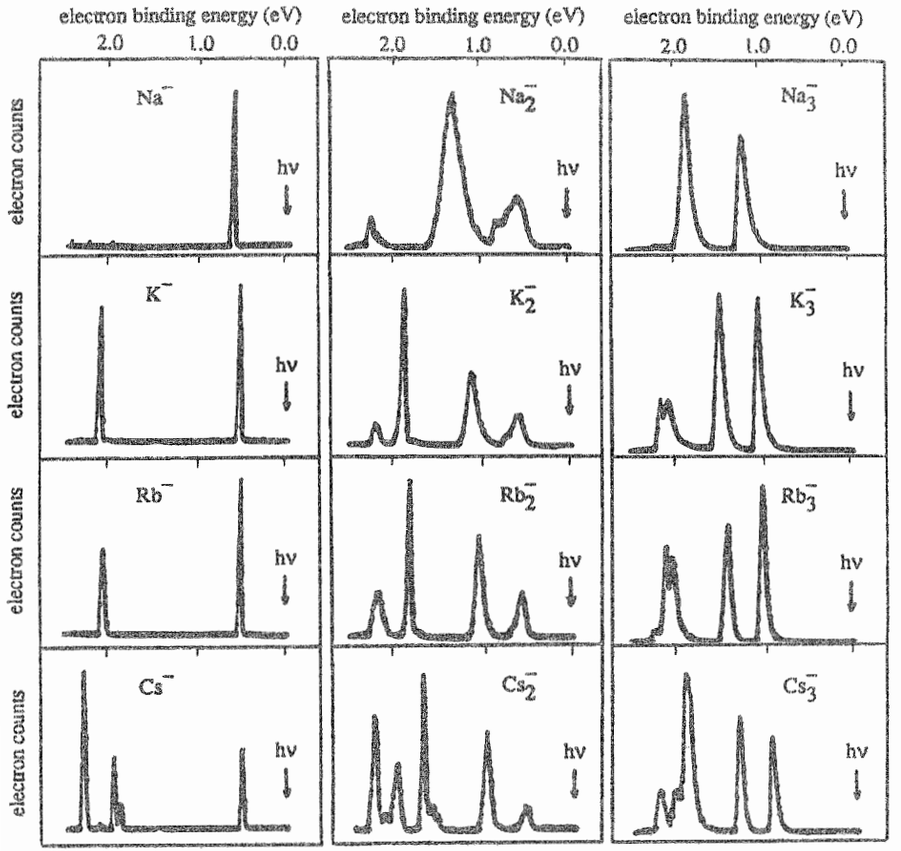


Figure 22. The photoelectron spectra of $Na^-_{n=1-3}$, $K^-_{n=1-3}$, $Rb^-_{n=1-3}$, and $Cs^-_{n=1-3}$



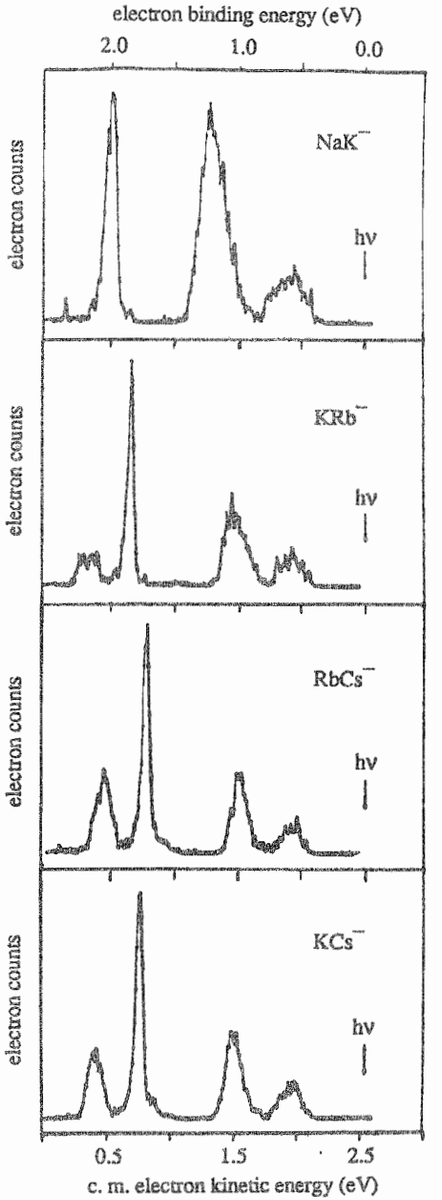


Figure 23. The photoelectron spectra of $NaK^-$, $KRb^-$, $RbCs^-$, and $KCs^-$

and their photoelectron spectra are presented in Figure 23. In all of these spectra, the individual peaks correspond to transitions from the ground state of the dimer or trimer anion to the various ground and excited electronic states of the corresponding neutral. In general, the vibrational states are too closely spaced to be resolved in this experiment, and the peaks in the spectra correspond to unresolved vibronic bands. The chemical kinship among the alkali dimers ($M_2$) is reflected by the similarity in the various spectral patterns, and this is also the case for the alkali trimers ($M_3$). As the alkalis become more massive, an increasing number of low lying electronic states are observed in the dimer and trimer anion spectra. This is due to screening effects which give rise to a contraction of the energies of the electronic states as the alkalis become heavier.

All of the dimer spectra have been assigned, the assignments being guided by available optical data and theoretical calculations (ref. 87). These spectra provide neutral dimer electronic state splittings (at the geometry of the anion), including those for a number of previously unobserved "optically dark" states. With state assignments in hand, optically-allowed transition energies were used to back-estimate the electron binding energies of the origin locations in the $X,M_2 \leftarrow X,M_2^-$ bands of these spectra. Using this procedure, the adiabatic electron affinities of the alkali dimers were determined to be 0.42 eV, 0.47eV, 0.48 eV, and 0.45 eV for $Na_2$, $K_2$, $Rb_2$, and $Cs_2$, respectively. These values follow the order $Na_2 < K_2 \cong Rb_2 > Cs_2$, consistent with theoretically predicted trends (ref. 88). Using these electron affinities in appropriate thermochemical cycles, anion dissociation energies were also calculated. As was the case in $Cu_2^-$, these dissociation energies are somewhat smaller than those of their corresponding neutrals.

In the case of the alkali trimers, there is probably a considerable geometry difference between the neutrals and their anions. While the neutral alkali trimers possess distorted triangular structures, the alkali trimer anions are thought to be linear (ref. 19, 89-93). The electron binding energy of the maximum in the highest electron kinetic energy peak in a given $M_3^-$ photoelectron spectrum corresponds to the transition energy between the ground state of the trimer anion and the ground electronic state of its corresponding neutral at the geometry of the anion, ie. this is the vertical detachment energy. The origin transition, from which the adiabatic electron affinity can be determined, lies to the low electron binding energy side of this peak. We were able to estimate the location of the origin on the side of this peak with the aid of calculations by Truhlar, Mead, and coworkers (ref. 94). These calculations provided the energy difference between linear and triangular



geometries of $Na_3$ and $K_3$. When we subtracted these energy increments from their corresponding vertical detachment energies, the resulting electron binding energies corresponded to inflection points (where the spectral intensities begin to rise rapidly) on the high kinetic energy sides of the origin-containing peaks. This provided confidence that these inflection points probably do correspond to the spectral origins, and that the spectral intensity to the high kinetic energy side of them is due only to hot bands. Using this method, the adiabatic electron affinities of $Na_3$ and $K_3$ were found to be 1.02 eV and 0.94 eV, respectively. Scaling the differences between vertical detachment energies and electron affinities to peak widths allowed the adiabatic electron affinities of $Rb_3$ and $Cs_3$ to be determined to be 0.91 eV and 0.87 eV, respectively. The electron affinities of the trimers were found to decrease as the alkali metals became more massive, in agreement with the trend predicted by Eades et al. (ref. 92).

### 5.4 Alkali Metal Cluster Series

The alkali metal cluster anions are particularly convenient systems to study with visible photons. The alkali metals have the lowest work functions of any metal, ranging from 2.42 eV for lithium to 2.14 eV for cesium. Since the highest possible value of a metal cluster electron affinity is equal to the work function of the metal, even very large alkali cluster anions can be photodetached with visible photons. In addition, for small alkali clusters with relatively low electron affinities, visible photons can be used in photodetachment experiments to access several of the low lying electronic states in neutral alkali clusters, providing considerable information about the evolution of electronic structure in alkali metal clusters.

The photoelectron spectra of the alkali metal cluster anions, $Na_{n=4,5}^-$ and $K_{n=4-7}^-$, are presented in Figure 24. The electron affinities of these clusters have been determined from these spectra, and a comparison of their electron affinities as a function of cluster size reveals two main trends (see Figure 25a). There is a gradual increase of the cluster electron affinity with increasing cluster size, beginning the evolution of the cluster electron affinity towards the bulk work function. Superimposed upon this overall increase in the electron affinity is an odd-even alternation, with clusters comprised of odd numbers of atoms generally having higher electron affinities than adjacent even sized clusters. The only exceptions to this pattern are $K_5$ and $K_6$, where the electron affinities

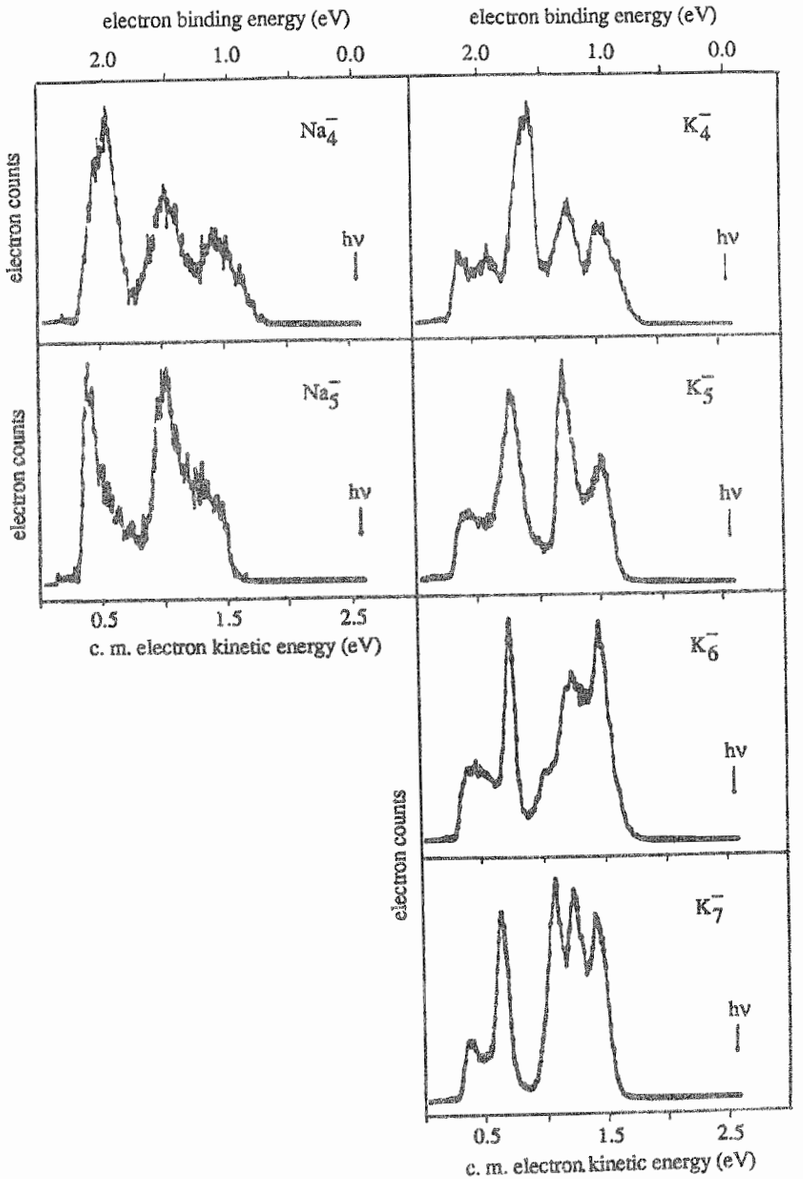


Figure 24. The photoelectron spectra of $Na^-_{n=4,5}$ and $K^-_{n=4-7}$



are the same for both species. All the cluster anion spectra are highly structured, this structure being due to the low lying electronic states of the corresponding neutral. It is interesting to note that even in the spectrum of the largest alkali cluster anion that we have studied, $K_7^-$, four (and the beginning of a fifth) low lying electronic states are clearly resolved. Also, for all the potassium and sodium cluster anions studied to date, the energy splittings between the ground and first excited states of their corresponding neutrals decrease rapidly with increasing cluster size.

Potassium ([Ar]$4s^1$) is electronically analogous to copper ([Ar]$3d^{10}4s^1$), inviting a number of comparisons between the two metal cluster series. While the electron affinity values of potassium and copper clusters of the same size are quantitatively rather different, plots of the electron affinity vs. cluster size for potassium and copper clusters (see Figure 25) reveal the same qualitative trend in each series. Both series exhibit gradually increasing electron affinities with increasing cluster size and an

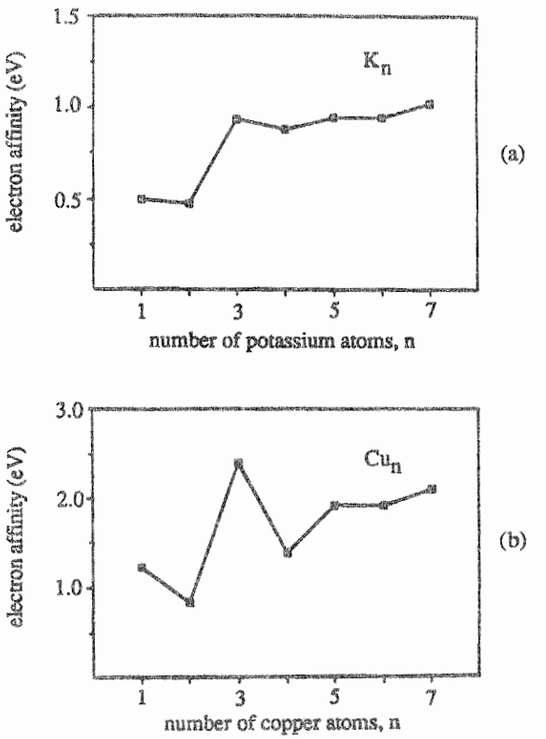


Figure 25. Electron afinities vs. cluster size for (a) $K_n$ and (b) $Cu_n$

odd-even alternation. In addition, the electron affinity trends of both metals track one another with specific similarities. For example, the largest single increase in electron affinity occurs between the dimer and trimer in both cases, while the electron affinity remains constant between the pentamer and hexamer in both. The qualitative trend in the size variation of this electronic property is strikingly similar in both copper and potassium.

Negative ion photoelectron spectra also reveal similarities in the electronic structure of neutral clusters of potassium and copper. In order to access the low lying electronic states of copper clusters, which are analogous to those we have observed in potassium clusters, it is necessary to record the photoelectron spectra of the copper cluster anions with near-ultraviolet photons. Figure 26 presents a comparison of copper and potassium cluster anion photoelectron spectra for the two cluster sizes where the pertinent data is available, ie. for $K_6^-$ and $Cu_6^-$ and for $K_7^-$ and $Cu_7^-$. The spectra of $Cu_6^-$ and $Cu_7^-$ were recorded by Smalley and coworkers (ref. 23) in the ultraviolet, while the spectra of $K_6^-$ and $K_7^-$ were recorded in our laboratory with visible photons. Reading the spectra to increasing electron binding energies (from right to left), one notes, in the spectra of both $K_6^-$ and $Cu_6^-$, a complex band with substantial sub-structure (see the bands labeled by features a and b in Figure 26), a gap, and then a peak (feature c in Figure 26). Within the complex band in both spectra, there are two unequal yet comparable-intensity peaks (a and b) with weaker features (some shoulders, some peaks) to either side of this doublet. We have not continued the comparison beyond peak c in the $K_6^-$ spectrum because there is an artificial decrease in signal beyond this point due to an unavoidable and rapid decrease in the transmission function of electrostatic electron energy analyzers at low electron kinetic energies. Making the same sort of comparison between $K_7^-$ and $Cu_7^-$, one encounters, in the $K_7^-$ spectrum, a triplet of resolved peaks (features a', b', and c'), a gap, and then a single peak (feature d'). In the case of the $Cu_7^-$ spectrum, one encounters a very broad band (labeled as c'b'a' in Figure 26), a gap, and a single peak (feature d'). Our suspicion that feature c'b'a' is actually comprised of several sub-peaks was confirmed very recently when Lineberger and coworkers (ref. 51) recorded the continuous beam ultraviolet photoelectron spectrum of $Cu_7^-$ and found that this feature can indeed be resolved into multiple peaks. These comparisons suggest a qualitative correspondence between the low lying electronic structure of copper and potassium clusters. Thus, it appears that both the electron affinity trends and the electronic state splitting patterns in both copper and potassium clusters are qualitatively similar.



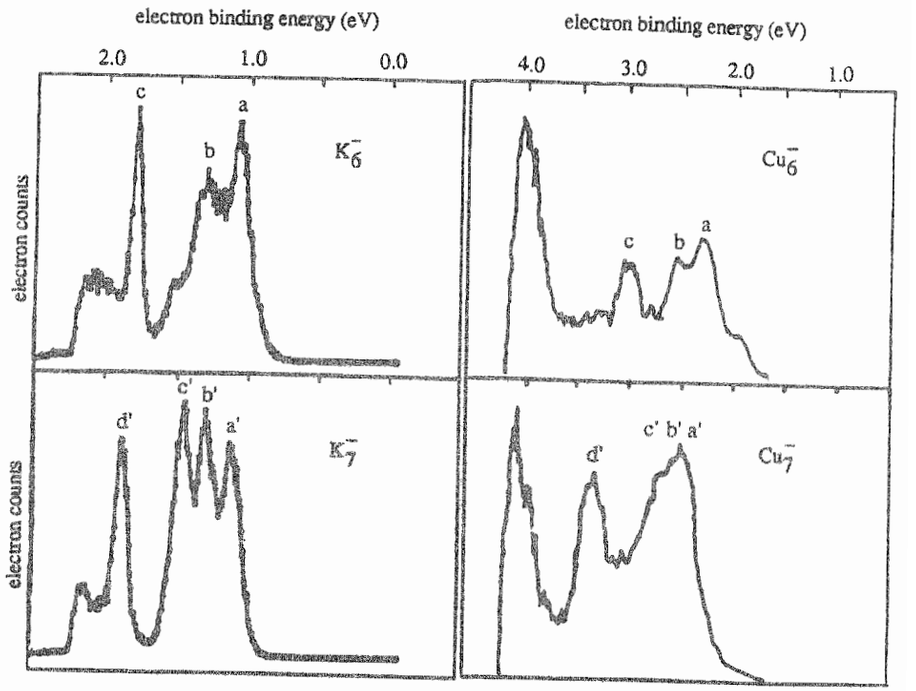


Figure 26. The photoelectron spectra of $K_{n=6,7}^-$ in the visible and $Cu_{n=6,7}^-$ in the ultraviolet

## 6. SUMMARY

This chapter has presented an overview of the cluster anions investigated by negative ion photoelectron spectroscopy, with particular emphasis given to those systems studied by continuous beam techniques. The three classes of negative cluster ions highlighted above include cluster anions with localized excess negative charges, cluster anions which exhibit excess charge delocalization, and metal cluster anions. Ion-molecule complexes are cluster anions in which the excess negative charge is localized on one component of the cluster, and the photoelectron spectra of these complexes reveal the identity of the cluster's sub-ion and the energetics of its interactions with its solvents, providing insight into anion solvation phenomena. Delocalized cluster anions were exemplified by the negative cluster ions of water. In these cases, the photoelectron spectra demonstrated an overall increase in

vertical detachment energies with increasing cluster size. For small water cluster anions, the spectra also provided a measure of the distortion that individual water sub-units experience due to the presence of excess electrons. The photoelectron spectra of metal cluster anions provide electron affinities and low lying electronic state splittings for the corresponding neutral clusters. Investigations of metal cluster anion series revealed the evolution of these electronic properties with increasing cluster size. Further studies of cluster anions by the technique of negative ion photoelectron spectroscopy will doubtlessly lead to a more thorough understanding of the chemistry and physics of clusters and cluster anions, as well as providing insight into solvation phenomena, the nature of excess electrons in fluids, and the metallic bulk state.

## ACKNOWLEDGEMENT

Most of the work from the authors' group, which was presented in this chapter, was supported by the National Science Foundation under grant #CHE 8511320. Our work with the smoke-ion source was supported primarily by the Semiconductor Research Corporation, and our collaboration with the Haberland group on water cluster anions was facilitated by a NATO grant.

## REFERENCES

* Author to whom correspondence should be addressed

1 P. Kebarle, in Ion-Molecule Reactions, ed. J. L. Franklin (Plenum, New York, 1972)

2. R. G. Keesee and A. W. Castleman, Jr., J. Phys. Chem. Ref. Data, 1986, 15, 1011

3. R. G. Keesee, N. Lee, and A. W. Castleman, Jr., J. Chem. Phys., 1980, 73, 2195

4. D. L. Albritton, At. Data and Nucl. Tables, 1978, 22

5. C. E. Klots and R. N. Compton, J. Chem. Phys., 1978, 69, 1636

6. K. H. Bowen, G. W. Liesegang, R. A. Sanders, and D. R. Herschbach, J. Phys.Chem., 1983, 87, 557

7. P. C. Cosby, J. H. Ling, J. R. Peterson, J. T. Moseley, J. Chem. Phys., 1976, 65, 5267

8. R. A. Beyer and J. A. Vanderhoff, J. Chem. Phys., 1976, 65, 2313

9. A. W. Castleman, Jr., D. E. Hunton, T. G. Lindeman, and D. N. Lindsay, Intl. J. Mass Spect. and Ion Phys., 1983, 47, 199

10. H.-S. Kim and M. Bowers, J. Chem. Phys., 1986, 85, 2718

11. S. Golub and B. Steiner, J. Chem. Phys., 1968, 49, 5191



12. H. Kistenmacher, H. Popkie, and E. Clementi, J. Chem Phys., 1973, 61, 5627

13. G. Chalasinski, R. A. Kendall, and J. Simons, J. Phys. Chem., 1987, 91, 6151

14. S. H. Fleishman and K. D. Jordan, J. Phys. Chem., 1987, 91, 1300

15. R. N. Barnett, U. Landman, C. L. Cleveland, and J. Jortner, J. Chem. Phys., 1988, 88, 4429

16. M. D. Newton, J. Phys. Chem., 1975, 79, 2795

17. J. Simons, Ann. Rev. Phys. Chem., 1977, 28, 15

18. C. F. Melius, T. H. Upton, and W. A. Goddard III, Solid State Comm., 1978, 28, 501

19. I. Boustani and J. Koutecky, J. Chem. Phys., 1988, 88, 5657

20. S. H. Yang, C L. Pettiette, J. Conceicao, O. Cheshnovsky, and R. E. Smalley, Chem. Phys. Lett., 1987, 139, 233

21. S. Yang, K. J. Taylor, M. J. Craycraft, J. Conceicao, C. L. Pettiette, O. Cheshnovsky, and R. E. Smalley, Chem. Phys. Lett., in press

22. L.-S. Zheng, C. M. Karner, P. J. Brucat, S. H. Yang, C. L. Pettiette, M. J. Craycraft, and R.E. Smalley, J. Chem. Phys., 1986, 85, 1681

23. C. L. Pettiette, S. H. Yang, M. J. Craycraft, J. Conceicao, R. T. Laaksonen, O.Cheshnovsky, and R. E. Smalley, J. Chem. Phys., 1988, 88, 5377

24. C. L. Pettiette and R. E. Smalley, 1988, private communication

25. L.-S. Zheng, P. J. Brucat, C. L. Pettiette, S. Yang, and R. E. Smalley, J. Chem. Phys., 1985, 83, 4273

26. Y. Liu, Q.-L. Zhang, F. K. Tittel, R. F. Curl, and R. E. Smalley, J. Chem. Phys., 1986, 85, 7434

27. O. Cheshnovsky, S. H. Yang, C. L. Pettiette, M. J. Craycraft, Y. Liu, and R. E. Smalley, Chem. Phys. Letter., 1987, 138, 119

28. L. A. Posey, M. J. DeLuca, and M. A. Johnson, Chem. Phys. Lett., 1986, 131, 170

29. L. A. Posey and M. A. Johnson, J. Chem. Phys., 1988, 88, 5383

30. M. J. DeLuca, B. Liu, and M. A. Johnson, J. Chem. Phys., 1988, 88, 5857

31. M. A. Johnson, 1988, private communication

32. R. B. Metz, T. Kitsopoulos, A. Weaver, and D. M. Neumark, J. Chem. Phys., 1988, 88, 1463

33. A. Webster, R. B. Metz, S. E. Bradforth, and D. M. Neumark, J. Phys. Chem., to be submitted

34. D. M. Neumark, 1988, private communication

35. G. Gantefor, K. H. Meiwes-Broer, and H. O. Lutz, Phys. Rev. A, 1988, 37, 2716

36. G. Gantefor, M. Gausa, K. H. Meiwes-Broer, and H. O. Lutz, Z. Phys. D, 1988, 9, 253

37. G. Gantefor, M. Gausa, K. H. Meiwes-Broer, and H. O. Lutz, Faraday Disc. Chem. Soc.,1988, 88

38. G. Gantefor, M. Gausa, K. H. Meiwes-Broer, and H. O. Lutz, Z. Phys. D, 1988, in press

39 K. H. Meiwes-Broer, 1988, private communication

40. C. R. Moylan, J. A. Dodd, and J. I. Brauman, Chem. Phys. Lett., 1985, 118, 38

41. C. R. Moylan, J. A. Dodd, C. C. Han, and J. I. Brauman, J. Chem. Phys., 1987, 86, 5350

42. D. M. Wetzel and J. I. Brauman, Chem. Rev., 1987, 87, 607

43. P. C. Engelking and W. C. Lineberger, J. Am. Chem. Soc., 1979, 101, 5569

44. A. E. Stevens, C. S. Feigerle, and W. C. Lineberger, J. Am. Chem. Soc., 1982, 104, 5026

45. T. M. Miller. D. G. Leopold, K. K. Murray, and W. C. Lineberger, Bull. Am. Phys. Soc., 1985, 30, 880

46. D. G. Leopold, T. M. Miller, and W. C. Lineberger, J. Am. Chem. Soc., 1986, 108, 178

47. D. G. Leopold and W. C. Lineberger, J. Chem. Phys., 1986, 85, 51

48. D. G. Leopold, J. Ho, and W. C. Lineberger, J. Chem. Phys., 1987, 86, 1715

49. D. G. Leopold, J. Almlof, W. C. Lineberger, and P. R. Taylor, J. Chem. Phys., 1988, 88, 3780

50. K. M. Ervin, J. Ho, and W. C. Lineberger, J. Chem. Phys., submitted

51. W. C. Lineberger, K. M. Ervin, and D. G. Leopold, 1988, private communication

52. M. R. Nimlos, L. B. Harding, and G. B. Ellison, J. Chem. Phys., 1987, 87, 5116

53. J. V. Coe, J. T. Snodgrass, C. B. Freidhoff, K. M. McHugh, and K. H. Bowen, J. Chem. Phys., 1985, 83, 3169

54. J. V. Coe, J. T. Snodgrass, C. B. Freidhoff, K. M. McHugh, and K. H. Bowen, Chem. Phys. Lett., 1986, 124, 274

55. J. V. Coe, J. T. Snodgrass, C. B. Freidhoff, K. M. McHugh, and K. H. Bowen, J. Chem. Phys., 1987, 87, 4302

56. J. T. Snodgrass, J. V. Coe, C. B. Freidhoff, K. M. McHugh, and K. H. Bowen, J. Chem. Phys., 1988, 88, 8014

57. K. H. Bowen and J. G. Eaton, in Proceedings of the International Workshop on the Structure of Small Molecules and Ions, (Jerusalem, Israel), in press

58. K. M. McHugh, Ph.D. Thesis, The Johns Hopkins University, (Baltimore, Maryland) 1988

59. J. T. Snodgrass, J. V. Coe, C. B. Freidhoff, K. M. McHugh, and K. H. Bowen, Faraday Disc. Chem. Soc., 1988, 88

60. R. J. Cellota, R. A. Bennett, and J. L. Hall, J. Chem Phys., 1974, 60, 1740

61. R. R. Corderman and W. C. Lineberger, Ann. Rev. Phys. Chem., 1979, 30, 347

62. J. V. Coe, J. T. Snodgrass, C. B. Freidhoff, K. M. McHugh, and K. H. Bowen, J. Chem. Phys., 1986, 84, 618

63. K. M. Ervin, J. Ho, and W. C. Lineberger, J. Phys. Chem., submitted

64. H. Haberland, H.-G. Schindler, and D. R. Worsnop, Ber. Bunsenges. Phys. Chem., 1984, 88, 270





65. K. M. McHugh, H. W. Sarkas, J. G. Eaton, C. R. Westgate, and K. H. Bowen, Z. Phys. D, 1988, in press

66. J. C. Kleingeld, S. Ingemann, J. E. Jalonen, and N. M. M. Nibbering, J. Am. Chem. Soc., 1983, 105, 2474

67. C. D. Ritchie and H. F. King, J. Am. Chem. Soc., 1968, 90, 838

68. J. Kalcher, P. Rosmus, and M. Quack, Can. J. Phys., 1984, 62, 1323

69. R. R. Squires, in Ionic Processes in the Gas Phase, ed. M. A. Amoster Ferreira, NATO Advanced Science Institutes Series, Series C (Reidel, Dordrecht, 1984), Vol. 118

70. A. J. Kos, P. von Rague Schleyer, J. A. Pople, and R. R. Squires, manuscript in preparation

71. D. Cremer and E. Kraka, J. Phys. Chem., 1986, 90, 33

72. H. Cardy, C. Larrieu, and A. Dargelos, Chem. Phys. Lett., 1986. 131, 507

73. K. Hirao and E. Kawai, J. Mol. Struct., 1987, 149, 391

74. J. V. Ortiz, J. Chem. Phys., 1987, 87, 3557

75. M. Gutowski, J. Simons, R. Hernandez, and H. L. Taylor, J. Phys. Chem., to be published

76. D.K. Bohme, R. S. Hemsworth, and H. W. Rundle, J. Chem. Phys., 1973, 59, 77

77. J.V. Coe, Ph.D. Thesis, The Johns Hopkins University, (Baltimore, MD) 1986

78. G.H. Lee, C. Ludewigt, J.G. Eaton, H. Haberland, and K.H. Bowen, to be published

79. A. Wallqvist, D. Thirumalai, and B.J. Berne, J. Chem. Phys., 1986, 85, 1583

80. U. Landman, R.N. Barnett, C.L. Cleveland, D. Scharf, and J. Jortner, J. Phys. Chem., 1987, 91, 4890

81. R. N. Barnett, U. Landman, C.L. Cleveland, and J. Jortner, Phys. Rev. Lett., 1987, 59, 811

82. M. D. Morse, Chem Rev. 1986, 86, 1049

83. I. Shim and K. A. Gingerich, J. Chem Phys., 1982, 77, 2490

84. I. Shim and K. A. Gingerich, J. Chem. Phys., 1983, 78, 5693

85. A. R. Miedema, Faraday Symp. Chem. Soc., 1980, 14, 136

86. L. Brewer and J. S. Winn, Faraday Symp. Chem. Soc., 1980, 14, 126

87. D. D. Konowalow and M. E. Rosenkrantz, in Metal Bonding and Interactions in High Temperature Systems, J. L. Gole and W. C. Stwalley, eds.(ACS Symposium Series 179 Washington D. C., 1982) p. 3

88. H. Partridge, D. A. Dixon, S. P. Walch, C. W. Bauschlicher, Jr., and J. L. Gole, J. Chem. Phys., 1983, 79, 1859

89. R. L. Martin and E. R. Davidson, Mol. Phys, 1978, 35, 1713

90. F. Cocchini, T. H. Upton, and W. Andreoni, J. Chem. Phys., 1988, 88, 6068

91. H.-O. Beckman, Chem. Phys.Lett., 1982, 93, 240

92. R. A. Eades, M. L. Hendewerk, R. Frey, D. A. Dixon, and J. L. Gole, J. Chem. Phys., 1982, 76, 3075

93. D. M. Lindsay, L. Chu, Y. Wang and T. F. George, J. Chem. Phys.,1987, 87, 1685

94. T. C. Thompson, G. Izmirlian, Jr., S. J. Lemon, D. G. Truhlar, and C. A. Mead, J. Chem. Phys., 1985, 82, 5597



SUBJECT INDEX